

# Specific Binding of Adamantane Drugs and Direction of Their Polar Amines in the Pore of the Influenza M2 Transmembrane Domain in Lipid Bilayers and Dodecylphosphocholine Micelles Determined by NMR Spectroscopy

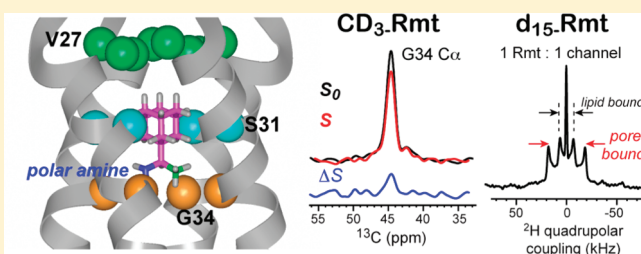
Sarah D. Cady,<sup>†</sup> Jun Wang,<sup>‡</sup> Yibing Wu,<sup>‡</sup> William F. DeGrado,<sup>\*,‡</sup> and Mei Hong<sup>\*,†</sup>

<sup>†</sup>Department of Chemistry, Iowa State University, Ames, Iowa 50011, United States

<sup>‡</sup>Department of Biochemistry & Biophysics, School of Medicine, and Department of Chemistry, University of Pennsylvania, Philadelphia, Pennsylvania 19104-6059, United States

Supporting Information

**ABSTRACT:** The transmembrane domain of the influenza M2 protein (M2TM) forms a tetrameric proton channel important for the virus lifecycle. The proton-channel activity is inhibited by amine-containing adamantyl drugs amantadine and rimantadine, which have been shown to bind specifically to the pore of M2TM near Ser31. However, whether the polar amine points to the N- or C-terminus of the channel has not yet been determined. Elucidating the polar group direction will shed light on the mechanism by which drug binding inhibits this proton channel and will facilitate rational design of new inhibitors. In this study, we determine the polar amine direction using M2TM reconstituted in lipid bilayers as well as dodecylphosphocholine (DPC) micelles.  $^{13}\text{C}$ - $^2\text{H}$  rotational-echo double-resonance NMR experiments of  $^{13}\text{C}$ -labeled M2TM and methyl-deuterated rimantadine in lipid bilayers showed that the polar amine pointed to the C-terminus of the channel, with the methyl group close to Gly34. Solution NMR experiments of M2TM in DPC micelles indicate that drug binding causes significant chemical shift perturbations of the protein that are very similar to those seen for M2TM and M2(18–60) bound to lipid bilayers. Specific  $^2\text{H}$ -labeling of the drugs permitted the assignment of drug–protein cross peaks, which indicate that amantadine and rimantadine bind to the pore in the same fashion as for bilayer-bound M2TM. These results strongly suggest that adamantyl inhibition of M2TM is achieved not only by direct physical occlusion of the channel, but also by perturbing the equilibrium constant of the proton-sensing residue His37. The reproduction of the pharmacologically relevant specific pore-binding site in DPC micelles, which was not observed with a different detergent, DHPC, underscores the significant influence of the detergent environment on the functional structure of this membrane protein.



## INTRODUCTION

The M2 protein of the influenza A virus is a membrane-spanning tetrameric proton channel responsible for a number of functions, including the acidification of the virion with concomitant uncoating of the viral RNA,<sup>1,2</sup> inhibition of autophagosome-lysosome fusion,<sup>3</sup> filamentous virus formation and viral membrane budding and scission.<sup>4–6</sup> This essential protein is the target of the adamantane class of anti-influenza drugs, amantadine (Amt) and rimantadine (Rmt). M2 has a modular structure<sup>7</sup> containing: (1) a short N-terminal region that is important for the protein's incorporation into the virion;<sup>8</sup> (2) a transmembrane (TM) helix required for tetramerization, drug-binding, and proton channel formation;<sup>7</sup> (3) an amphiphilic cytoplasmic helix required for filamentous virion formation, budding, and ESCRT-independent membrane scission;<sup>4–6</sup> and (4) a C-terminal tail that interacts with the matrix protein, M1.<sup>9</sup>

Mutagenesis and electrophysiological measurements of full-length M2 in *oocytes* showed that drug-resistant mutations occur

at pore-lining residues (Leu26, Val27, Ala30, Ser31, Gly34) of the N-terminal portion of the TM helix.<sup>10–13</sup> These residues line the Amt-binding site, as seen in the crystal structure of Amt-bound M2TM.<sup>14</sup> Solid-state NMR (SSNMR) distance measurements between  $^{13}\text{C}$ -labeled M2TM and  $^2\text{H}$ -labeled Amt in lipid bilayers<sup>15</sup> showed that Amt exclusively bound to this site when the drug was present at the stoichiometric concentration relative to the number of protein tetramers. However, when Amt was in excess to the channels and formed a significant fraction of the lipid bilayer (>5 mol % of the phospholipids), it also showed dipolar interactions with Asp44 on the surface of the four-helix bundle.<sup>15</sup> This peripheral interaction had previously been seen in the solution NMR structure of M2(18–60) in mixed micelles consisting of 7.5: 1 DHPC/Rmt, which was equivalent to a 200-fold excess of drug relative to tetramers.<sup>16</sup> The pharmacological

Received: March 27, 2010

Published: March 07, 2011

relevance of the two sites was addressed by a series of electrophysiological studies<sup>10–12</sup> that assessed the drug sensitivities of reverse-engineered viruses in which either the peripheral site or the pore site was mutated. These studies and other functional assays<sup>17</sup> supported the high-affinity binding site within the pore to be the pharmacologically relevant binding site.

There are several possible mechanisms of M2 inhibition by Amt and Rmt in the pore. First, the location of the drug physically occludes the pore, as in the classical mechanism of channel blockers. Second, the M2 TM domain is structurally plastic, switching between multiple conformational states during proton conduction as well as triggered by other environmental factors.<sup>14,18–23</sup> Any drug that locks the protein into a single form will inhibit the structural transitions required for ion conduction, particularly if the drug-stabilized conformational state is a nonconducting resting state. Indeed, channel-blockers have been known to be able to act in part via conformational selection.<sup>24,25</sup> Finally, drug-binding was observed to strongly perturb the acid dissociation constants ( $pK_a$ 's) of the proton-sensing His37 residues<sup>26,27</sup> through a mechanism that has not yet been fully understood.

To elucidate the mechanism with which Amt and Rmt perturb the His37  $pK_a$ , it is important to determine the direction of the polar moiety of these drugs. Both Amt and Rmt contain a hydrophobic adamantyl cage connected to a polar moiety, which is an amine in Amt and ethylamine in Rmt. Perturbation of the His37  $pK_a$  can be understood if the polar group points down toward the C-terminus of the channel rather than up toward the N-terminus.<sup>28</sup> However, the amine direction of these drugs has not been directly determined. In a number of computational studies, energetically reasonable solutions for the amine up or down directions were found, and the amine direction varied with pH and mutation of the pore-lining residues.<sup>29–34</sup> Experimental efforts to determine the amine direction are also inconclusive: the crystal structure of the Amt-bound M2TM did not have sufficient resolution (3.5 Å) to unambiguously define the amine direction, although the C-terminus-facing direction was favored.<sup>14</sup> The recent high-resolution SSNMR study based on cage-perdeuterated Amt ( $d_{15}$ -Amt) could not probe the amine direction.<sup>15</sup> Therefore, the polar group direction of the adamantyl drugs in the pore remains an open question; its elucidation will be important for the design of second-generation compounds against drug-resistant variants of M2.

The purpose of this study is 2-fold. First, we determine the polar group direction of the adamantyl drugs in the pore using solid-state NMR  $^{13}\text{C}$ – $^2\text{H}$  dipolar coupling measurements in lipid bilayers. We use methyl-deuterated Rmt as the probe for the amine direction of the drugs in the pore, and  $^2\text{H}$  quadrupolar spectra of cage-perdeuterated Rmt ( $d_{15}$ -Rmt) to determine the tilt angle of Rmt in the pore as well as in the lipid bilayer. Second, these solid-state NMR measurements were complemented by isotope-edited solution NMR experiments that show that M2TM exhibits the same specific drug-binding site in DPC micelles as in lipid bilayers. The parallel solution and solid-state NMR experiments were motivated by the fact that the previous solution NMR study of M2(18–60) in DHPC micelles<sup>16</sup> did not observe a pore-bound drug. By comparing the NMR spectra of M2TM in micelles and in native-like lipid bilayers, we wish to address whether detergent micelles in general perturb the pore binding site,<sup>35</sup> or whether it is the specific combination of the longer M2 construct with the DHPC micelle in the previous solution NMR study<sup>16</sup> that abolished the pore binding site. The choice of the TM constructs for this study, rather than the longer

construct containing both the TM helix and the cytoplasmic helix, is based on the now large body of evidence showing that the cytoplasmic helix is not required for Amt-sensitive proton channel activities. First, electrophysiological measurements of M2TM in oocytes<sup>7</sup> with careful quantification of the surface expression level of the peptide showed that the single-channel conductivity of M2TM is within a factor of 2 of that of the full-length protein, which revised the conclusions of an earlier study.<sup>36</sup> Several liposome assays also showed that M2TM conductance was 50–100% that of the full-length protein or the cytoplasmic-helix-containing construct.<sup>7,37</sup> Second, numerous biophysical studies showed that M2TM was both necessary and sufficient for tetramerization in detergent micelles,<sup>14,38</sup> and the thermodynamics of tetramerization<sup>7,28,39–45</sup> reproduces the unusual  $pK_a$  of the essential His37 in the full-length protein.<sup>7,27</sup> Third, a large number of low-resolution biophysical studies, including fluorescence,<sup>41</sup> isothermal titration calorimetry,<sup>7</sup> and surface plasmon resonance,<sup>46</sup> demonstrated that M2TM is capable of binding adamantyl drugs, and drug binding inhibits proton translocation through M2TM channels in vesicles.<sup>7,27</sup>

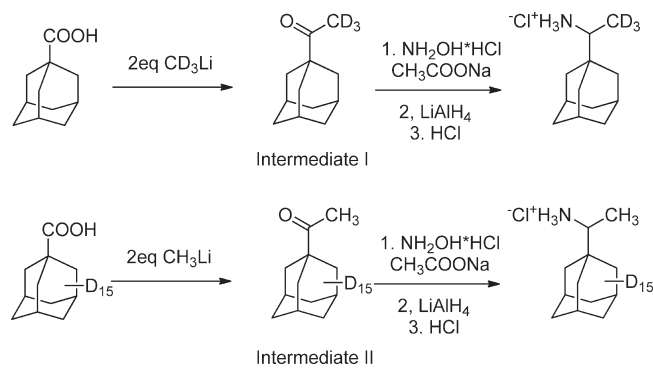
Instead of mediating proton conductance, the latest reports make it clear that the cytoplasmic helix mediates budding and release of the virus from infected cells.<sup>4–6</sup> Simultaneous mutation of five hydrophobic residues (F47, F48, I51, Y52, and F55) to Ala in this helix gave rise to viruses that are defective in budding but fully capable of proton conductance as the wild-type protein.<sup>5</sup> Site-directed spin-labeling EPR<sup>47</sup> and oriented solid-state NMR data<sup>48</sup> showed that the cytoplasmic helix is oriented parallel to and packed closely with the plane of the bilayer, stabilized by hydrophobic interactions between residues on one face of the cytoplasmic helix and the lipid bilayer. These findings revise the separate water-soluble helical bundle structure obtained earlier by solution NMR.<sup>16</sup>

## MATERIALS AND METHODS

The M2 transmembrane domain spans roughly residues 22–46. We used two slightly different M2TM constructs in this study: M2TM(22–46) by chemical synthesis and M2TM(19–49) by recombinant expression.

**Optimized Synthesis Procedure for M2TM(22–46).** Because of the requirements for a large quantity of isotopically labeled peptides and the hydrophobic nature of M2TM, we developed an optimized procedure that delivers crude peptide with >80% purity. Problems encountered in obtaining high-yields and purity included aspartamide formation at residue 44 and slow coupling near the center of the chain. M2TM(22–46) with uniformly  $^{13}\text{C}$ ,  $^{15}\text{N}$ -labeled V27, A30, and G34 (VAG-M2TM) was synthesized using Fmoc chemistry at elevated temperature (75 °C for both coupling and deprotection) in a semiautomated Quest synthesizer using Rink Amide Chemmatrix resin (Matrix Innovation, Inc., Canada). Coupling reagents were 5 equiv amino acid, 5 equiv HCTU, 10 equiv DIEA in NMP for 5 min coupling. Five percent piperazine and 0.1 M HOBr in DMF were used as the deprotection solution in order to minimize aspartamide formation. The peptide was cleaved from the resin using 95% TFA, 2.5% Tris, 2.5%  $\text{H}_2\text{O}$  and precipitated from ether after removal of TFA. Ether was decanted after centrifugation and the peptide was washed with cold ether again. The final peptide was dissolved in 50% B' (59.9% 2-propanol, 30% acetonitrile, 10%  $\text{H}_2\text{O}$ , and 0.1% TFA) and 50% A (99.9%  $\text{H}_2\text{O}$ , 0.1% TFA) and purified by preparative C4 reverse phase HPLC with a linear gradient of 70% B' to 85% B'. The peptide was eluted at 78% B'. The purity and identity of the peptide was confirmed by analytical HPLC (>98% purity) and MALDI–MS. Calculated MS: 2782.38; Observed MS: 2782.90.

**Scheme 1. Synthetic Scheme for CD<sub>3</sub>-Rimantadine and d<sub>15</sub>-Rimantadine**



**Expression of <sup>15</sup>N-Labeled and <sup>15</sup>N, <sup>13</sup>C-Labeled M2TM(19–49).** Uniformly <sup>15</sup>N-labeled or <sup>15</sup>N, <sup>13</sup>C double labeled M2TM(19–49) for solution NMR experiments were obtained by expressing the full-length protein in minimal medium enriched with 1 g/L <sup>15</sup>N NH<sub>4</sub>Cl or 1 g/L <sup>15</sup>N NH<sub>4</sub>Cl and 4 g/L <sup>13</sup>C glucose.<sup>7</sup> The protein was reconstituted in octylglucopyranoside (OG) micelles and digested with TPCK-treated trypsin (Thermo Fisher), following a modification of the method described previously<sup>40</sup> and in the Supporting Information. The peptide was purified to homogeneity by reverse-phase HPLC, and its purity and identity confirmed by analytical HPLC, MALDI-MS, and high-resolution ESI-MS. Analytical data are provided in the Supporting Information.

**Synthesis of Two Deuterated Rimantadine Compounds.** 1-Adamantane-d<sub>15</sub>-carboxylic acid was purchased from C/D/N isotopes, Inc. CD<sub>3</sub>Li in diethyl ether was purchased from Sigma-Aldrich. 1D <sup>1</sup>H and <sup>13</sup>C NMR spectra were recorded on a DMX-360 NMR spectrometer. Chemical shifts are reported in parts per million (ppm) and referenced to the residual solvent (CD<sub>3</sub>OD or CDCl<sub>3</sub>) signals. The following abbreviations were used in reporting the NMR spectra: s, singlet; t, triplet; m, multiplet; p, pentet. All reactions were carried out under a N<sub>2</sub> atmosphere unless otherwise stated. HPLC grade solvents were used for all reactions. Column chromatography was performed using silica gel (230–400 mesh). ESI mass spectra were obtained on a 3200 Q Trap LC/MS/MS system (Applied Biosystems).

**Synthesis of CD<sub>3</sub>-Rimantadine.** Intermediate I (Scheme 1): A solution of 0.5 M CD<sub>3</sub>Li (44 mL, 22 mmol) in diethyl ether was added dropwise to an ice-bath cooled solution of 1-adamantane carboxylic acid (1.8 g, 10 mmol) in diethyl ether (50 mL) with stirring. The mixture was stirred at 0 °C for 30 min, and then continued at ambient temperature for 4 h. The reaction mixture was slowly poured into a vigorously stirring solution of 1 N HCl (100 mL) in ice water bath. Ether (50 mL) was added to the solution and the layers were separated; the aqueous layer was further extracted three times with diethyl ether. The combined ether layers were extracted with aqueous NaHCO<sub>3</sub> and dried with MgSO<sub>4</sub>. The solvent was removed under reduced pressure and the crude product was purified by silica gel flash column chromatography (5–10% ethyl acetate/hexane) to give intermediate I as a white solid (1.57 g, Yield: 88%). <sup>1</sup>H NMR (360 MHz, CDCl<sub>3</sub>) δ 2.06 (br s, 3H), 1.79–1.65 (m, 12H); <sup>13</sup>C NMR (90 MHz, CDCl<sub>3</sub>) δ 214.21, 46.63, 38.40, 36.73, 28.12. The calculated mass for C<sub>12</sub>H<sub>15</sub>OD<sub>3</sub> (M + H)<sup>+</sup> is 182.3; found, 182.5.

A solution of Intermediate I (181 mg, 1 mmol), NH<sub>2</sub>OH·HCl (208.5 mg, 3 mmol), and CH<sub>3</sub>COONa (328.1 mg, 4 mmol) in anhydrous EtOH (5 mL) was heated to reflux for 2 h. The solvent was removed under reduced pressure and the residue was dissolved in CH<sub>2</sub>Cl<sub>2</sub> and extracted with H<sub>2</sub>O twice. The organic layer was dried with MgSO<sub>4</sub> and the solvent was removed under reduced pressure to give the oxime intermediate. Without further purification, the oxime was dissolved in anhydrous THF (10 mL) and cooled to 0 °C with an ice–water bath. LiAlH<sub>4</sub> (0.4 g, 10.5 mmol) was added portion-wise to the stirring mixture. The solution was warmed to ambient temperature and heated to reflux for 4 h. The reaction was quenched by sequential addition of 0.4 mL of H<sub>2</sub>O, 0.4 mL of 15% NaOH solution, and 1.2 mL of H<sub>2</sub>O. The resulting slurry was filtered and the solvent was removed by rotary-evaporation under reduced pressure. Four molar HCl in 1,4-dioxane (1 mL) was added to the oily residue and the solvent was removed again under reduced pressure to give a white solid crude product, which was subsequently purified by silica gel flash column chromatography (10–20% CH<sub>3</sub>OH/CH<sub>2</sub>Cl<sub>2</sub>) to yield CD<sub>3</sub>-rimantadine as a yellow solid (164 mg, Yield: 75%). <sup>1</sup>H NMR (360 MHz, CD<sub>3</sub>OD) δ 2.86 (br s, 1H), 2.03 (br s, 3H), 1.74–1.60 (m, 12H); <sup>13</sup>C NMR (90 MHz, CD<sub>3</sub>OD) δ 57.90, 38.74, 37.65, 35.29, 29.30. The calculated mass for C<sub>12</sub>H<sub>19</sub>ND<sub>3</sub> (M + H)<sup>+</sup> is 183.3; found, 183.7. (The <sup>13</sup>C NMR experiment did not use <sup>2</sup>H decoupling so the signal of the CD<sub>3</sub> carbon was not detected due to splitting by deuterons.)

**Synthesis of d<sub>15</sub>-Rimantadine.** The synthesis procedure of d<sub>15</sub>-rimantadine was the same as described above except starting with 1-adamantane-d<sub>15</sub>-carboxylic acid and CH<sub>3</sub>Li.

Intermediate II: <sup>1</sup>H NMR (360 MHz, CDCl<sub>3</sub>) δ 2.09 (s, 3H); <sup>13</sup>C NMR (90 MHz, CDCl<sub>3</sub>) δ 214.16 (s), 46.04 (s), 37.50 (p, J = 18.0 Hz), 35.40 (p, J = 18.0 Hz), 27.12 (t, J = 18.9 Hz), 24.34 (s). The calculated mass for C<sub>12</sub>H<sub>14</sub>OD<sub>15</sub> (M + H)<sup>+</sup> is 194.3; found, 194.3.

D<sub>15</sub>-Rimantadine: <sup>1</sup>H NMR (360 MHz, CD<sub>3</sub>OD) δ 2.91 (s, 3H), 1.26 (s, 3H); <sup>13</sup>C NMR (90 MHz, CD<sub>3</sub>OD) δ 58.06 (s), 37.63 (p, J = 18.0 Hz), 36.37 (p, J = 18.0 Hz), 34.89 (s), 28.27 (t, J = 18.9 Hz), 13.65 (s). The calculated mass for C<sub>12</sub>H<sub>7</sub>ND<sub>15</sub> (M + H)<sup>+</sup> is 195.3; found, 195.8.

**Solution NMR Experiments.** Solution NMR spectra were recorded at 313 K on a Varian INOVA 500 MHz spectrometer with a conventional probe, and 600 and 900 MHz spectrometers equipped with cryogenic <sup>1</sup>H{<sup>13</sup>C, <sup>15</sup>N}-triple resonance probes. <sup>15</sup>N TROSY-HSQC, <sup>13</sup>C HSQC, 2D H(N)CA, 2D (H)C(C)H-TOCSY spectra<sup>49</sup> were collected for backbone and side chain resonance assignment of <sup>15</sup>N, <sup>13</sup>C-labeled VAG-M2TM. 2D (<sup>13</sup>C)-NOESY spectra with a 200 ms mixing time were acquired to identify <sup>1</sup>H–<sup>1</sup>H NOE between the peptide and Amt or Rmt. Spectra were processed with the program NMRPipe.<sup>50</sup> Prior to Fourier transformation, time domain data were multiplied by sine square bell window functions shifted by 90° and zero-filled once. <sup>1</sup>H chemical shifts were referenced to the residual water signal while <sup>13</sup>C and <sup>15</sup>N chemical shifts were indirectly referenced to DSS.

**Rimantadine Titration and Analysis of Binding Isotherm.** A sample of 0.94 mM M2(19–49) in DPC (peptide/detergent molar ratio 1:50) was titrated stepwise with Rmt at 313 K and <sup>15</sup>N–<sup>1</sup>H HSQC spectra recorded on a Bruker DMX-600 spectrometer. The integrated intensity for the cross-peaks associated with the drug-bound form of V27, V28, A30, I32, I35, G34, L38, I39, and I40 were determined and plotted against the concentration of drug added. The integrated intensities were normalized such that the maximal value was 1.0 for each resonance, and the entire data set was analyzed by the method of nonlinear least-squares fitting to a binding isotherm using the following equation:

$$\frac{[I_{\text{obs}}]}{[I_{\text{sat}}]} = \frac{K_D [\text{Tetra}]_T \times N + [\text{Rmt}]_T - \sqrt{(K_D + [\text{Tetra}]_T \times N + [\text{Rmt}]_T)^2 - 4[\text{Tetra}]_T \times N \times [\text{Rmt}]_T}}{2[\text{Tetra}]_T \times N} \quad (1)$$

in which  $I_{\text{obs}}$  and  $I_{\text{sat}}$  are the intensities at a given drug concentration and at saturating drug concentration;  $[\text{Tetra}]_T$  is the total peptide

concentration divided by four,  $[\text{Rmt}]_T$  is the total drug concentration,  $N$  represents the number of drugs per tetramer, and  $K_D$  is the

dissociation constant. To explore the stoichiometry, we performed a number of calculations. Initially,  $N$  was either fixed to 1 or 4, and the value of  $K_D$  was treated as a variable. Only a value of  $N = 1$  gave a reasonable fit to the data. Alternatively,  $N$  and  $K_D$  were both allowed to vary, which resulted in a value of  $N = 0.88 \pm 0.04$ . We attribute the small difference from 1.0 to error in determining the peptide concentration and/or incomplete reconstitution of the sample. Because  $[\text{Tetra}]_T$  is significantly greater than  $K_D$  for the interaction, the precise value of this parameter could not be determined. Satisfactory fits to the data were obtained in successive curve-fits in which this value was less than or equal to approximately  $5 \mu\text{M}$  (Supporting Information).

**Membrane-Bound M2TM Samples for Solid-State NMR.** Residue-specifically labeled M2TM(22–46) for SSNMR experiments was synthesized by PrimmBiotech (Cambridge, MA) and purified to >95% purity. Uniformly  $^{13}\text{C}$ ,  $^{15}\text{N}$ -labeled amino acids were incorporated at residues Val27, Ser31, Gly34, and Asp44 (VSGD-M2TM). Unlabeled peptides were used for static  $^2\text{H}$  quadrupolar echo experiments that detect Rmt dynamics and orientation. M2TM(22–46) was reconstituted into 1,2-dimyristoyl-sn-glycero-3-phosphocholine (DMPC) vesicles by OG dialysis.<sup>51</sup> The final peptide/lipid molar ratio was 1: 8. A pH 7.5 phosphate buffer (10 mM  $\text{Na}_2\text{HPO}_4/\text{NaH}_2\text{PO}_4$ , 1 mM EDTA, 0.1 mM  $\text{NaN}_3$ ) was used to prepare the lipid vesicle solutions. The protein–lipid solutions were dialyzed at 4 °C for 3 days with 5 to 6 buffer changes to remove the detergent. Protein–lipid precipitates usually formed after 1 day of dialysis. The proteoliposome mixtures were centrifuged at 150 000g to obtain ~40% hydrated membrane pellets for SSNMR experiments.  $d_{15}\text{-Rmt}$  or  $\text{CD}_3\text{-Rmt}$  was dissolved in water and directly titrated into the membrane pellet. For  $^{13}\text{C}$ – $^2\text{H}$  REDOR experiments,  $\text{CD}_3\text{-Rmt}$  was added at a ratio of 1 drug/tetramer or 5 drugs/tetramer, which corresponded to drug/lipid molar ratios of 1: 60 or 1: 12, respectively. For static  $^2\text{H}$  NMR experiments,  $d_{15}\text{-Rmt}$  was added to unlabeled M2TM at 1 drug/tetramer and 4 drugs/tetramer ratios. Excess water after the addition of Rmt was evaporated by placing the rotor uncapped in a desiccator at room temperature for several hours.

**Solid-State NMR Experiments.** Static  $^2\text{H}$  quadrupolar echo experiments were carried out on a 14.1 T wide-bore solid-state NMR spectrometer (Bruker Biospin) operating at a  $^2\text{H}$  Larmor frequency of 92.12 MHz using a double-resonance 4 mm  $^1\text{H}$ / $^2\text{H}$  probe. The quadrupole-echo experiment involved a pre-echo delay of 40–50  $\mu\text{s}$ , an 8  $\mu\text{s}$  shorter post-echo delay, and a  $^2\text{H}$  90° pulse length of 3.8  $\mu\text{s}$ . The time signal was left-shifted appropriately to capture the echo maximum to give Fourier-transformed spectra with flat baselines. The spectra were measured from 243 to 303 K. The number of scans ranged from 30 000 to 150 000.

$^{13}\text{C}$ -detected and  $^2\text{H}$ -dephased REDOR experiments were carried out using a triple-resonance 4 mm  $^1\text{H}$ / $^{13}\text{C}$ / $^2\text{H}$  magic-angle-spinning (MAS) probe on a 9.4 T wide-bore SSNMR spectrometer (Bruker Biospin) operating at a  $^{13}\text{C}$  resonance frequency of 100.71 MHz and a  $^2\text{H}$  frequency of 61.48 MHz. The samples were spun under 4250 Hz MAS at 243 K, where the protein was immobile but the drug remained dynamic. The REDOR experiment involved a single selective  $^{13}\text{C}$  180°-pulse in the center of the mixing period and multiple  $^2\text{H}$  180° pulses of 12.4  $\mu\text{s}$  every half a rotor period. This version of the REDOR experiment removes  $^{13}\text{C}$ – $^{13}\text{C}$  scalar coupling and thus gives long  $^{13}\text{C}$   $T_2$  relaxation times, which allows the detection of dephasing effects at long mixing times. An alternative REDOR version containing a single  $^2\text{H}$  composite 90°–90°–90° pulse and multiple  $^{13}\text{C}$  hard 180° pulses was also conducted at one mixing time to confirm the dipolar dephasing (data not shown). Although the second experiment produces quantitative dephasing,<sup>15</sup> the complex dynamics of the rotating methyl group attached to a uniaxially diffusing adamantyl cage prohibits distance quantification from the dephasing curve; thus, we did not attempt to measure multiple REDOR time points using the latter experiment.

Static  $^2\text{H}$  lineshapes of  $d_{15}\text{-Rmt}$  were simulated using MATLAB and the software EXPRESS.<sup>52</sup> For each molecular orientation of Rmt, a 4:1

area ratio of two couplings with a 1:3 splitting ratio was maintained to represent the equatorial and axial deuterons of the adamantyl cage. Since the effect of uniaxial diffusion on the quadrupolar coupling is known analytically, the coupling values were directly inputted into the EXPRESS program to generate the Pake patterns. Fitting the measured spectrum yielded the ratio between different orientations of Rmt in the channel pore versus in the bilayer.

## ■ RESULTS AND DISCUSSION

**Amt and Rmt Binding to M2TM in DPC Micelles.** We measured the location of Amt and Rmt bound to M2TM in DPC micelles using solution NMR. To evaluate the effect of drug binding on the structure of the M2TM tetramer, we first examined uniformly  $^{15}\text{N}$ -labeled and  $^{13}\text{C}$ ,  $^{15}\text{N}$ -labeled M2TM(19–49), which was prepared by controlled proteolysis of the native, full-length protein expressed in bacteria. We explored the spectroscopic properties of M2TM(19–49) using DPC micelles, because the tetramerization, affinity, and stoichiometry of drug binding to various fragments of M2 had been extensively evaluated in this detergent micelle.<sup>7,40,41</sup> Thus, it was possible to choose conditions where M2TM(19–49) was predominantly tetrameric. In addition to Amt and Rmt, we also examined a spiro-piperidine inhibitor WJ10, which had been shown to bind to M2TM strongly and perturb its conformation in a similar fashion as the adamantyl drugs.<sup>53</sup> Figure 1a shows the  $^{15}\text{N}$ – $^1\text{H}$  HSQC spectrum of M2TM(19–49) in the absence of drug, which showed limited peak dispersion. Addition of the spiro-piperidine inhibitor<sup>53</sup> and Amt (Figure 1b, Figure S1) into the sample resulted in the appearance of a new set of significantly sharper resonances in slow exchange with the resonances of the unbound species. Confirming the observations of SSNMR,<sup>21</sup> drug binding stabilized a slowly exchanging conformer that is in low abundance in the absence of the drug (Figure S2).

The drug-bound conformation shows large chemical shift changes of the resonances throughout the peptide relative to the unbound form. In particular, drug binding perturbed the chemical shifts of Val27, Ala30 and Gly34 (Figures S3, S4) as well as the aromatic resonances of His37 and Trp41 away from their frequencies typically seen in proteins (Figure 1, Figure S2). The changes are especially pronounced in the  $^1\text{H}$  dimension, in which the dispersion of the amide  $^1\text{H}$  chemical shifts increased by 2-fold (Figure 1), indicating the formation of a uniquely folded tertiary structure. The increased spectral dispersion is similar to that seen upon titration of the drug into M2TM<sup>51,54</sup> or M2(18–60)<sup>23</sup> in phospholipid bilayers, but contrasts with the minimal changes seen when the drug was titrated into M2(18–60) in DHPC micelles.<sup>16</sup>

To determine the stoichiometry of binding, we monitored the intensity of the drug-bound peaks as a function of the total Rmt concentration. The  $^{15}\text{N}$ – $^1\text{H}$  cross peaks of nine different amides were sufficiently well dispersed to allow unambiguous measurement of their intensities. A plot of the normalized integrated peak volume relative to the volume seen at saturating drug concentration increased linearly with drug concentration until one equivalent of drug per tetramer has been added, after which no further increase was observed. Figure 2a shows curves generated assuming a stoichiometry of either one or four drugs per tetramer; a satisfactory fit is obtained only for the 1 drug/tetramer complex. To further examine the stoichiometry and affinity of the complex, the data were analyzed using eq 1. Least-squares analysis of the

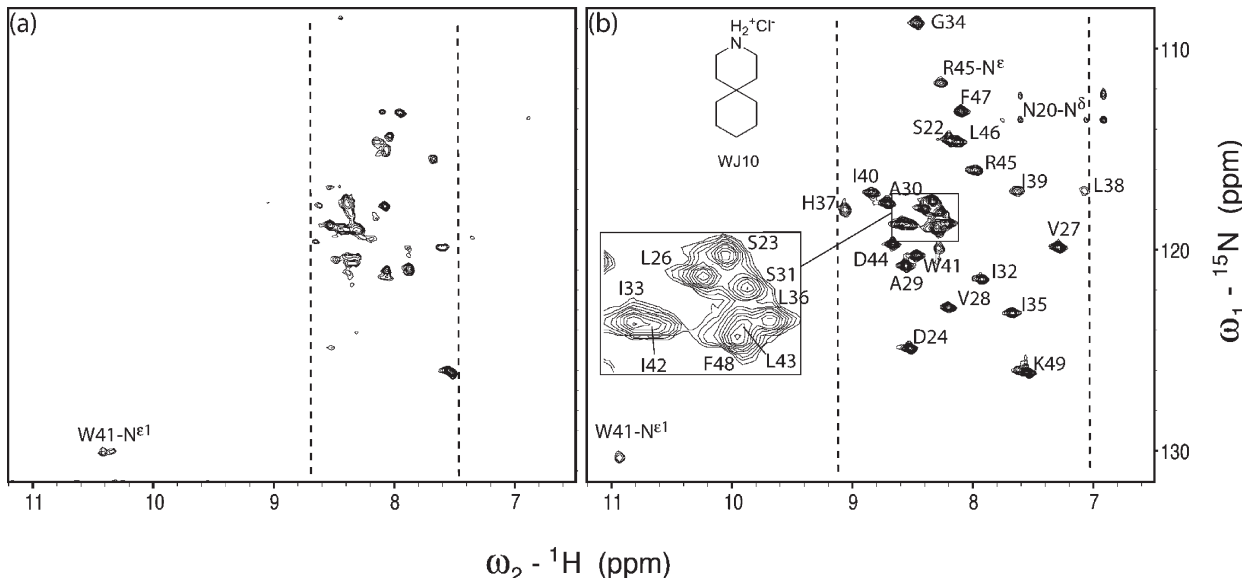


**Figure 1.** 2D  $^{15}\text{N}$  TROSY-HSQC spectra of 1 mM (monomer concentration) M2TM(19–49) in the absence (a) and presence (b) of 2.5 mM WJ10. The spectra were measured at 313 K in 100 mM DPC micelle (50 mM sodium phosphate, pH 7.5, in 10%  $\text{D}_2\text{O}$  and 90%  $\text{H}_2\text{O}$ ) on a cryoprobe-equipped Varian INOVA 600 MHz NMR. Upon drug binding, the signals became better dispersed in the  $^1\text{H}$  dimension, and the improved line shape and uniformity of the linewidths indicate that the bound protein adopts a well-folded conformation. Assignments are labeled for the bound protein and inset shows an expanded view of part of the spectrum. The chemical structure of spiro-piperidine WJ10 ( $\text{IC}_{50} = 0.92 \mu\text{M}$ ) is shown in the spectrum on the right. For comparison, Amt has an  $\text{IC}_{50} = 16 \mu\text{M}$ .<sup>53</sup>

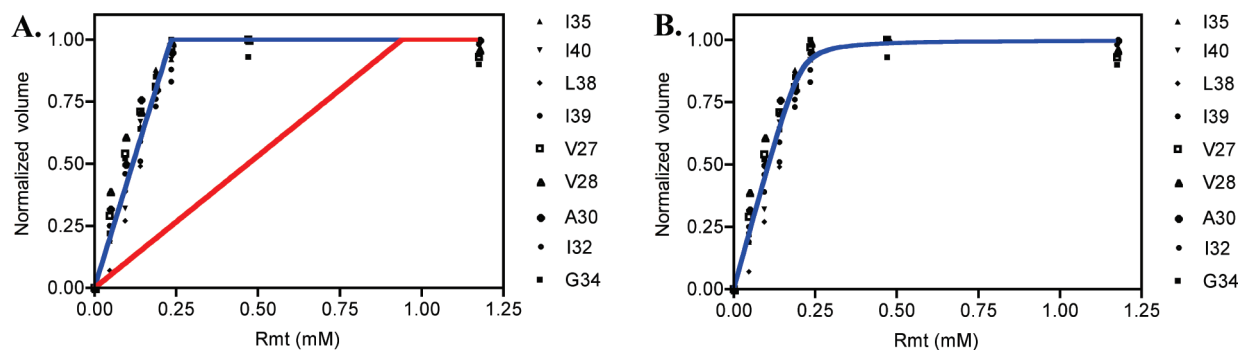


**Figure 2.** Titration of 0.94 mM M2(19–49) (monomer concentration) by Rmt. The intensities of the indicated peaks from the  $^{15}\text{N}$   $^1\text{H}$  HSQC spectra are plotted as a function of Rmt concentration. The curve has a well-defined break at a molar ratio of one drug/tetramer shown in blue in panel A. The corresponding titration curve expected for tight binding of the drug in a 4 drugs/tetramer complex is shown in red. Panel B shows a least-squares fit, in which the stoichiometry and  $K_D$  were allowed to vary, as described in Materials and Methods. The curve was generated using best-fit parameters of  $0.88 \pm 0.04$  drug/tetramer and  $K_D = 3.9 \mu\text{M}$ . A sensitivity analysis (Figure S1) showed that the value of  $K_D$  was less than or equal to  $5 \mu\text{M}$  under these conditions, although it was not possible to obtain a precise value for  $K_D$  under these conditions. Data were collected at 313 K, pH 7.5, in DPC (protein/DPC ratio 1:50), 50 mM sodium phosphate buffer.

data indicated a stoichiometry close to 1 drug/tetramer ( $N = 0.9$ ). Because the titration was conducted at protein concentrations that are significantly above the  $K_D$ , it is difficult to obtain a precise value for this parameter. However, a sensitivity analysis (Figure S5) indicated that the value of  $K_D$  was less than or equal to  $5 \mu\text{M}$  under these conditions.

The specific location of Amt and Rmt in M2TM(22–46) was investigated using  $^{13}\text{C}$ -edited NOESY experiments. Because of the difficulty of conducting half-filtered experiments on fast-relaxing proteins in detergent micelles, we opted to measure difference spectra of the peptides in the presence of deuterated versus protonated drugs. Two sets of experiments were carried out to detect NOE signals between the drug and

$^{13}\text{C}$ -labeled residues, one comparing protonated versus perdeuterated Amt, and the other comparing protonated versus  $\text{CD}_3$ -labeled Rmt. Three residues in the pore binding site—Val27, Ala30 and Gly34—were labeled with  $^{13}\text{C}$  and  $^{15}\text{N}$ . Any NOEs from the protonated drugs to these residues that disappear upon deuteration represent specific drug–protein interactions. Figure 3 shows  $^{13}\text{C}$ -edited NOESY spectra for protonated and perdeuterated Amt. The drugs were not  $^{13}\text{C}$ -labeled; thus, the only cross-peaks associated with the drug must result from interactions with the  $^{13}\text{C}$ -labeled residues of the protein, and drug–drug NOEs cannot exist in the spectra. We observed a strong NOE cross-peak at  $\sim 0.7$  ppm in the direct dimension and  $\sim 1.6$  ppm in the indirect dimension, which was assigned to the

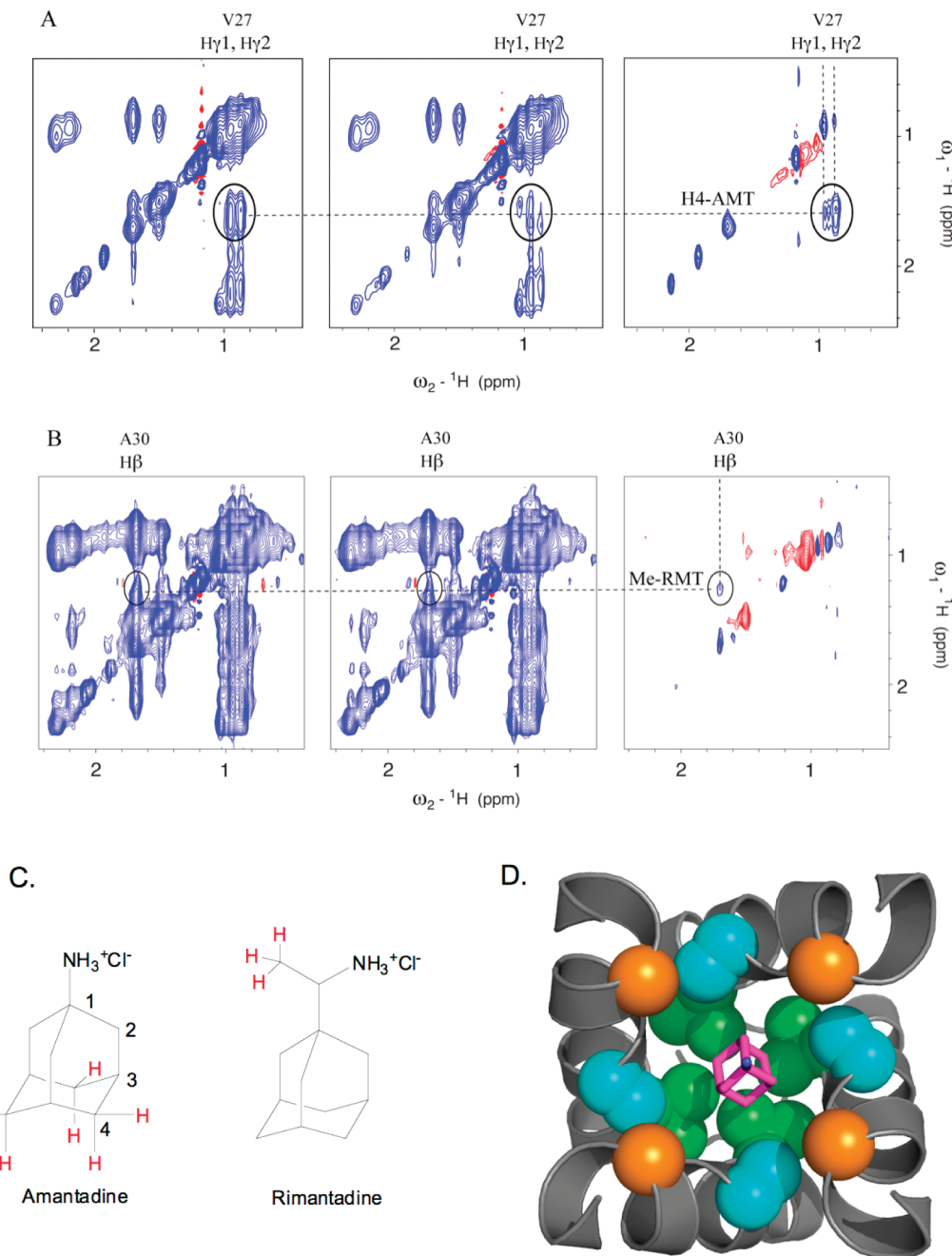


**Figure 3.** Upfield region of 2D <sup>13</sup>C-edited <sup>1</sup>H NOESY spectra with 200 ms mixing of <sup>13</sup>C, <sup>15</sup>N-labeled VAG-M2TM with 2 equiv Amt (A) and Rmt (B). The left spectra are those of protonated drugs, and the middle spectra are from samples containing perdeuterated Amt and methyl-deuterated Rmt. The right spectra are the difference between the left and middle spectra. (C) The protons that show NOE cross peaks with M2 are highlighted in red in the Amt and Rmt structures. Spectra in (A) and (B) were recorded on a 500 MHz and a 600 MHz spectrometer, respectively. The concentrations were 2 mM peptide, 100 mM DPC, 1 mM Amt or Rmt, and pH 7.5 phosphate buffer. The methyl groups of Val were not stereospecifically assigned. (D) The structure of Amt bound in the channel pore in the crystal structure of M2TM,<sup>14</sup> viewed from the C-terminal end. Shown in balls are Gly34 C $\alpha$  (orange), Val27 side chains (green), and Ala30 side chains (cyan). The hydrophobic adamantyl cage (magenta) interacts extensively with the Val27 side chains, while the polar group (blue) points to the C-terminus in the crystal structure.

$\gamma\text{CH}_3$  of Val27 and the C4 methylene protons of Amt (Figure S6). This cross peak indicates that the hydrophobic cage of Amt points up to the N-terminus while the polar amine points down, consistent with the SSNMR result of cage-perdeuterated Amt<sup>15</sup> and the X-ray structures<sup>14</sup> of the complex, in which the side chain of Val27 forms a hydrophobic lid of the binding site, interacting with the apolar portion of the drug. It is also

consistent with the fact that Val27 forms closer contacts with the adamantyl cage than Ala30 in both the crystal and SSNMR structures (Figure 3D).

To probe the polar group direction of Rmt in the pore, we performed the same <sup>13</sup>C-edited NOESY experiments of the peptide bound to CD<sub>3</sub>-labeled Rmt versus protonated Rmt. Figure 3B shows a weak NOE cross peak between the  $\beta\text{CH}_3$

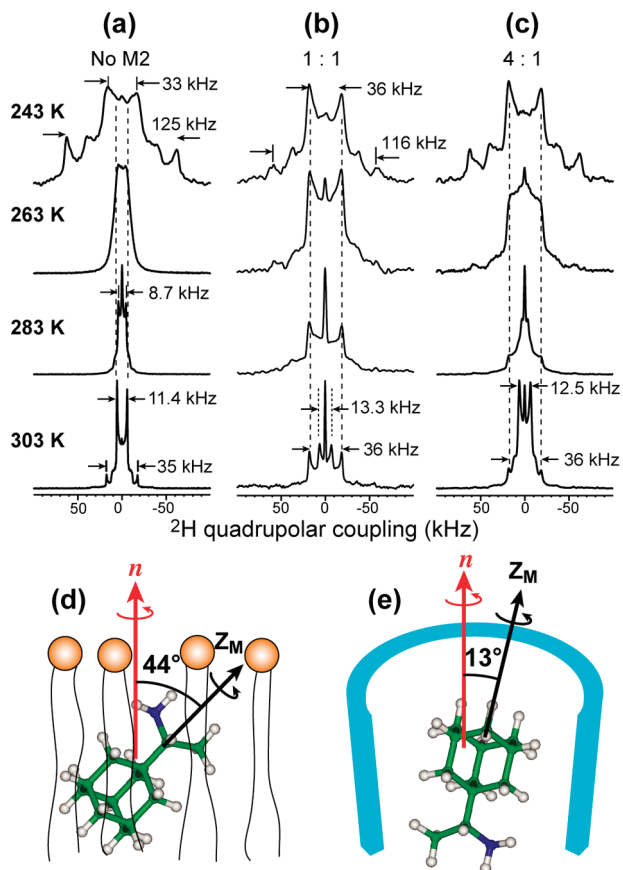


**Figure 4.** Static  $^2\text{H}$  quadrupolar echo spectra of  $d_{15}\text{-Rmt}$  for determining the tilt angle of the adamantyl cage in M2TM (residues 22–46) channels versus lipid bilayers. (a)  $d_{15}\text{-Rmt}$  bound to DMPC bilayers without the protein. (b)  $d_{15}\text{-Rmt}$  bound to M2TM in DMPC bilayers with 1 drug/tetramer. (c)  $d_{15}\text{-Rmt}$  bound to M2TM with 4 drugs/tetramer. (d) One of the two degenerate orientations of  $d_{15}\text{-Rmt}$  in lipid bilayers at 303 K. (e) Orientation of  $d_{15}\text{-Rmt}$  in M2TM channels at 303 K.

of Ala30 and Rmt CH<sub>3</sub>. Taken together, these NOESY difference experiments indicate that both Amt and Rmt bind in the channel pore with the amine pointing toward the C-terminus in DPC-bound M2TM tetramers.

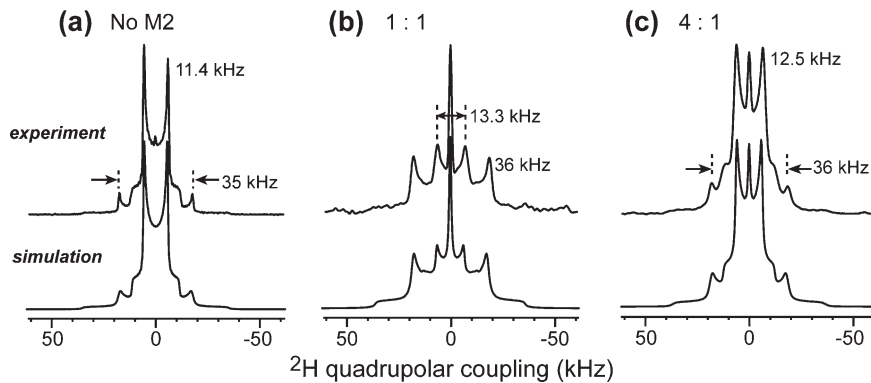
**Adamantyl Cage Orientations of Rmt in DMPC-Bilayer-Bound M2TM(22–46).** To determine the Rmt orientation and dynamics in M2TM reconstituted in lipid bilayers, which better represent the virus envelope, we measured the  $^2\text{H}$  spectra of  $d_{15}\text{-Rmt}$ . Rimantadine consists of a rigid adamantyl cage attached to an ethylamine. Similar to Amt, the adamantyl cage has a 3-fold symmetric axis  $Z_M$ . Three axial C–D bonds are parallel to  $Z_M$  while 12 equatorial C–D bonds lie at 70° or 110° from  $Z_M$ . Fast uniaxial rotation or C<sub>N</sub> jumps ( $N \geq 3$ ) of the cage around  $Z_M$  results in quadrupolar splittings of 40 and 125 kHz with a 4:1 intensity ratio. If the drug undergoes additional fast diffusion about the bilayer normal  $\vec{n}$  with a tilt angle  $\theta_{nM}$  from the molecular axis, then both equatorial and axial couplings will be further scaled by an order parameter,  $S_{\text{mol}} = (3 \cos^2 \theta_{nM} - 1)/2$ .<sup>55,56</sup> Apart from the axial rotation, wobble of the molecular axis from the bilayer normal is an alternative motional model that is particularly relevant when  $S_{\text{mol}}$  is large, corresponding to when the molecular axis lies close to the motional axis. This diffusion in a cone model scales the couplings according to  $S_{\text{mol}} =$

$\cos \theta_{nM}(1 + \cos \theta_{nM})/2$ . For simplicity, below we assume the axial rotation model in the analysis of the  $^2\text{H}$  quadrupolar spectra. While the adamantyl cage moiety is identical between Rmt and Amt, the different polar functionality between the two drugs can affect the molecular orientation, as we show below.

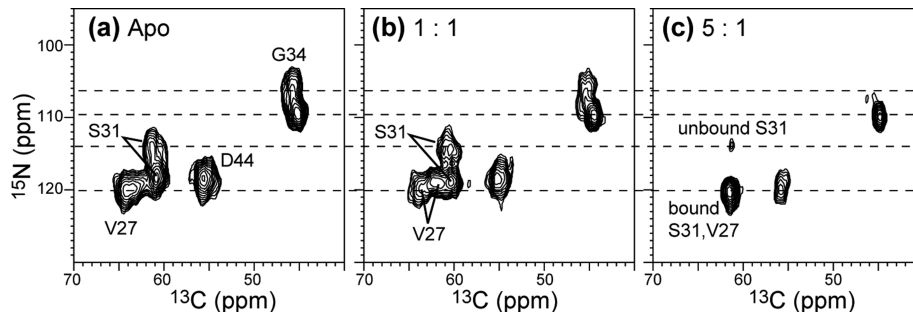
Figure 4 shows the  $^2\text{H}$  spectra of  $d_{15}\text{-Rmt}$  under varying drug/tetramer ratios from 243 to 303 K. Three membrane samples were examined: Rmt bound to DMPC bilayers in the absence of M2TM, in the presence of a stoichiometric number of tetramer (1 drug/tetramer), and in 4-fold excess of the number of channels (4 drugs/tetramer). At 243 K, all three samples exhibited quadrupolar splittings of ~35 and ~120 kHz, consistent with the frequency ratio expected when the adamantyl cage uniaxially rotates around its own molecular axis. The slight reduction of the splittings from 40 and 125 kHz give  $S_{\text{mol}} \approx 0.9$ , which indicates that  $Z_M$  is tilted by 13° from the bilayer normal in the axial rotation model. These 243 K spectra of Rmt are identical to the spectra of  $d_{15}\text{-Amt}$  at the same temperature.<sup>15</sup>

When the membranes were warmed to the liquid-crystalline phase at 303 K, the  $^2\text{H}$  spectra differed for the three samples. The lipid-only sample showed two splittings of 11.4 and 35 kHz, which corresponded to  $S_{\text{mol}}$  of  $\pm 0.28$ , indicating that the adamantyl cage is tilted from the bilayer normal by 44° (or 67°) at physiological temperature (Figure 4d). Simulation of the 303 K spectrum confirmed the intensity and frequency ratios of the underlying Pake patterns that represent the equatorial and axial deuterons (Figure 5a). The 44° tilt angle of lipid-bound Rmt is significantly larger than the 37° found for Amt.<sup>15</sup> We hypothesize that the bifurcated ethylamine interacts differently with the bilayer in order to better position the polar moiety with respect to the negatively charged phosphate groups on the membrane surface; thus, the molecule adopts a different tilt angle from Amt.

When a stoichiometric amount of M2 tetramers was present, the 303 K spectrum changed qualitatively from the lipid-only sample: the 36 kHz splitting of the equatorial deuterons at 243 K persisted to 303 K across the membrane phase transition, and dominated the spectral intensity (Figure 4b). The persistence of this large coupling at high temperature is similar to what was observed for Amt<sup>15</sup> and indicates that a significant fraction of Rmt cannot deviate from the upright orientation due to confinement by the channel (Figure 4e), and the drug is well isolated from the disordered liquid-crystalline membrane. In addition to the 36-kHz splitting, a 13.3 kHz splitting and an isotropic peak were detected in the stoichiometric spectrum at 303 K. The former corresponds to  $S_{\text{mol}} = 0.33$  or  $\theta_{nM} = 42^\circ$ , which can be attributed to Rmt in the lipid bilayer, since the amphipathic drug has affinity to both the lipids and the aqueous pore of the channel. The fact that the splitting is 2 kHz larger than the 11.4 kHz value seen in the lipid-only sample (Figure 4a) translates to only a small (~2°) reduction in the tilt angle, because the order parameter has the highest angular sensitivity at 45°. The isotropic peak, which was also observed for Amt<sup>15</sup> may result from randomly tumbling drug that escaped into the inter-bilayer aqueous phase, or from pore-bound drug tilted at the magic angle (54.7°) from the channel axis. The fractions of the three components were found by simulation (Figure 5b) to be 63%:27%:10% for the 13°-tilted channel-bound component, the 42°-tilted lipid-bound component (13.3 kHz), and the isotropic component. The lipid-bound fraction of 27% is higher than the 10% fraction for Amt,<sup>15</sup> suggesting that Rmt has higher affinity for the membrane than Amt under the molar ratios used in these solid-state NMR samples.



**Figure 5.** Simulations of the  $^2\text{H}$  spectra of  $d_{15}\text{-Rmt}$  at 303 K. (Top row) Experimental spectra reproduced from Figure 4. (Bottom row) Simulated spectra. (a)  $d_{15}\text{-Rmt}$  bound to DMPC bilayers without M2. Simulation used a 4:1 area ratio of the small and large couplings, consistent with the number of equatorial and axial deuterons in the adamantyl cage. (b)  $d_{15}\text{-Rmt}$  bound to M2 at 1 drug/tetramer. Simulated spectrum used an area ratio of 63%/27%/10% for the 36 kHz, 13.3 kHz, and isotropic components, which represent the pore bound, lipid bound and isotropic drugs. (c)  $d_{15}\text{-Rmt}$  bound to M2(22–46) at 4 drugs/tetramer. Simulated spectrum used an area ratio of 13%/83%/4% for the 36 kHz, 12.5 kHz and isotropic components.



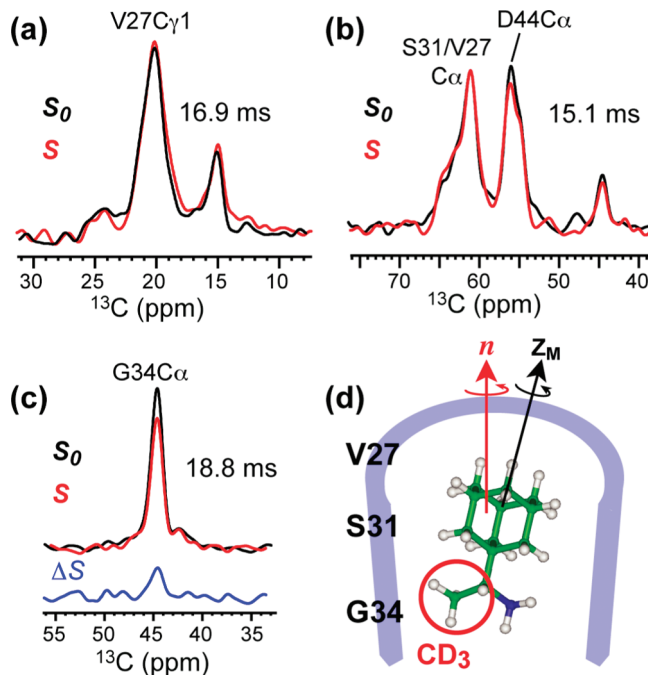
**Figure 6.** 2D  $^{15}\text{N}$ - $^{13}\text{C}$  correlation spectra of Val27, Ser31, Gly34 and Asp44-labeled M2TM in DMPC bilayers without and with Rmt. (a) The spectrum of drug-free peptide. (b) The spectrum of the 1 drug/tetramer sample. (c) The spectrum of the 5 drugs/tetramer sample. Ser31 and Gly34  $^{15}\text{N}$  chemical shift increases and Val27 C $\alpha$  chemical shift decreases upon drug binding.

Figure 4c shows the  $^2\text{H}$  spectra when Rmt is in 4-fold excess to the M2TM tetramers and accounting for 8 mol % of the lipid membrane. The 303 K spectrum is now dominated by a 12.5 kHz splitting and a small 36-kHz component for the equatorial deuterons. Thus, the excess drug adopts a similarly tilted orientation as the lipid-bound drug in the absence of the protein, while the drug inside the pore retained the same upright orientation as in the stoichiometric sample.<sup>15</sup> Simulation (Figure 5c) yielded a ratio of 13%:83%:4% for the 36 kHz, 12.5 kHz, and isotropic components.

Taken together, these  $^2\text{H}$  spectra indicate that the majority of the first equivalent of Rmt adopts a nearly upright orientation in the pore of the channel, identical to Amt. Excess Rmt has a very tilted orientation of 42–43° from the bilayer normal, which is very similar to the 44° tilt of the drug in the lipids in the absence of the protein. Compared to Amt, Rmt has a slightly different equilibrium constant between the high-affinity pore-binding site and the low-affinity lipid-binding site, which is likely a result of the different hydrophobicity and size of the two drugs.

**Binding Locations and Polar Group Direction of Rmt in the M2TM Pore.** Protein chemical shift perturbation provides independent evidence of ligand binding sites. To confirm the binding locations inferred from the  $^2\text{H}$  spectra and to compare M2-Rmt interactions with M2-Amt interactions, we measured the  $^{13}\text{C}$  and  $^{15}\text{N}$  chemical shifts of several key residues in M2TM. Ser31, Val27 and Gly34 are the respective center and boundaries

of the pore binding site for Amt,<sup>15,51</sup> while Asp44 probed the interaction of the drug with the lipid-exposed binding site. Figure 6 shows 2D  $^{15}\text{N}$ - $^{13}\text{C}$  correlation spectra of VSGD-M2TM(22–46) in the absence and presence of Rmt. The drug-free peptide shows two Ser31 peaks and two Gly34  $^{15}\text{N}$  peaks, whose relative intensities changed with titration of the drug: the downfield  $^{15}\text{N}$  peaks of each residue increased in intensity upon Rmt binding. The bound Ser31  $^{15}\text{N}$  peak is 6 ppm downfield from the unbound peak, while the bound Gly34  $^{15}\text{N}$  peak is 3 ppm downfield from the unbound peak. These peak displacements are very similar to those observed for Amt-bound M2TM,<sup>15,51</sup> strongly suggesting that Rmt also binds to the N-terminal pore near Ser31. The fact that the bound Ser31 conformation is already present in the drug-free state indicates that Rmt shifts the conformational equilibrium of the protein to the bound state rather than inducing an entirely new conformation. This observation is consistent with the concept of conformational selection by ligands, which has been documented for many globular proteins<sup>57</sup> and has also been reported for M2TM.<sup>18</sup> The Val27 C $\alpha$  chemical shift decreased by 2.5 ppm upon Rmt binding. In comparison, the Asp44  $^{15}\text{N}$  chemical shift did not change between the apo sample and the stoichiometric sample (both at 118.4 ppm), but increased by 1.5 ppm (at 119.9 ppm) in the sample containing excess Rmt. Thus, only excess drug affects the Asp44 conformation, providing strong evidence that the first equivalent of drug binds elsewhere from Asp44.



**Figure 7.**  $^{13}\text{C}\{^2\text{H}\}$  REDOR spectra of DMPC-bound M2TM with  $\text{CD}_3\text{-Rmt}$  at 5 drugs/tetramer. Intensity difference between the control ( $S_0$ , black) and dephased spectra ( $S$ , red) indicate proximity of the  $^{13}\text{C}$ -labeled residues to the deuterated methyl group. (a) 16.9 ms REDOR spectra of Val27  $\text{C}\gamma 1$ , showing  $S/S_0 = 1.02 \pm 0.04$ . (b) 15.1 ms REDOR spectra of Ser31  $\text{C}\alpha$  ( $S/S_0 = 1.02 \pm 0.03$ ) and Asp44  $\text{C}\alpha$  ( $S/S_0 = 0.89 \pm 0.03$ ). (c) Gly34  $\text{C}\alpha$  REDOR spectra at 18.8 ms, with  $S/S_0 = 0.81 \pm 0.04$ . The difference spectrum is shown in blue. (d) Schematic of rimantadine structure in the pore, with the polar amine pointing to the C-terminus and the adamantan cage tilted by  $\sim 13^\circ$ .

$^{13}\text{C}\{^2\text{H}\}$  REDOR experiments using  $\text{CD}_3\text{-Rmt}$  provided definitive proof of not only the binding location of the drug, but also the direction of the amine in the pore. If the ethylamine points to the N-terminus of the channel, significant REDOR effect will be expected for Val27 side chains, whereas if the amine points to the C-terminus, significant REDOR dephasing should be detected for Gly34. Since the Rmt  $^2\text{H}$  spectra and the 2D  $^{15}\text{N}-^{13}\text{C}$  spectra of the protein with varying drug concentrations both indicate that excess Rmt does not remove the high-affinity pore binding site, we focused the  $^{13}\text{C}\{^2\text{H}\}$  REDOR experiment on the 5 drugs/tetramer sample. Figure 7 shows the REDOR control ( $S_0$ ) and dephased ( $S$ ) spectra measured with a single  $^{13}\text{C}$  180° pulse and multiple  $^2\text{H}$  pulses.<sup>58</sup> Val27  $\text{C}\gamma 1$  exhibited no dephasing at 16.9 ms, and the combined Ser31 and Val27  $\text{C}\alpha$  peak at 61.4 ppm also showed no dephasing ( $S/S_0 = 1.02 \pm 0.03$  at 15.1 ms), indicating that both  $^{13}\text{C}$ -labeled residues are outside dipolar contact of the deuterated methyl group. In contrast, significant dephasing was observed for Gly34  $\text{C}\alpha$  with an  $S/S_0$  value of  $0.81 \pm 0.04$  at 18.8 ms. Thus, the REDOR spectra indicate unambiguously that the ethylamine lies near Gly34 and points to the C-terminus of the channel, in the direction of the His37.

Figure 7b also shows moderate dephasing of Asp44  $\text{C}\alpha$  to  $0.89 \pm 0.03$  at 15.1 ms, indicating that, at a lipid/drug molar ratio of 6.4:1, Rmt is in dipolar contact with the surface-exposed Asp44, similar to Amt.<sup>15</sup> Both Rmt and Amt are amphiphilic molecules and partition into the membrane–water interface of lipid bilayers,<sup>59</sup> at approximately the same depth as Asp44. Thus, drug

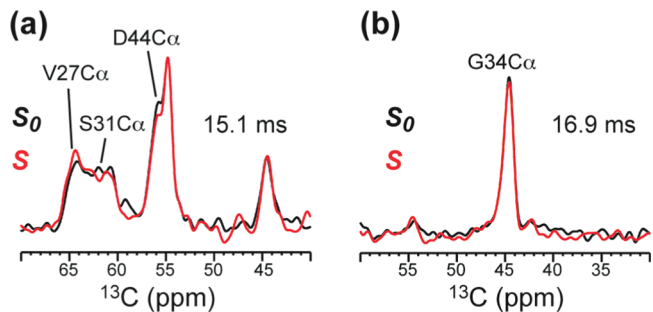


**Figure 8.**  $^{13}\text{C}\{^2\text{H}\}$  REDOR spectra of M2TM in DMPC bilayers with  $\text{CD}_3\text{-Rmt}$  at 1 drug/tetramer. (a) 15.1 ms REDOR spectra.  $S/S_0$  values are  $1.02 \pm 0.04$  for Val27  $\text{C}\gamma 1$ ,  $1.00 \pm 0.19$  for Ser31  $\text{C}\alpha$ , and  $0.92 \pm 0.08$  for Asp44  $\text{C}\alpha$ . (b) 16.9 ms REDOR spectra of Gly34  $\text{C}\alpha$ .  $S/S_0 = 0.94 \pm 0.07$ .

binding to Asp44 can be attributed to the high concentration of the drugs in the bilayer and the preference of the drugs for the glycerol interfacial region of the membrane.

Additional REDOR experiments of the 1 drug/tetramer sample (Figure 8) exhibited no significant dephasing for the four residues within experimental uncertainty, which is expected for Val27, Ser31 and Asp44. The lack of strong dephasing for Gly34 is partly due to incomplete occupancy of the drug in the pore: 27% of the Rmt is in the bilayer and 10% has vanishing quadrupolar coupling (Figure 4), thus,  $\sim 37\%$  of the drug is unable to cause dipolar dephasing. In addition, we suspect the peptide conformation may slightly differ between low and high drug concentrations due to changes in the membrane viscosity and lateral pressure, such that the height of the  $\text{CD}_3$  group may be slightly different between stoichiometric and excess drug concentrations. Previously we did not observe different REDOR dephasing between the stoichiometric and drug-excess complexes between  $d_{15}\text{-Amt}$  and M2TM.<sup>15</sup> However,  $d_{15}\text{-Amt}$  contains a large number of deuterons distributed over a 2.2 Å vertical distance, which would minimize the effects of small displacements of the drug in the pore. In contrast, the current  $\text{CD}_3\text{-Rmt}$  contains only three deuterons concentrated in a small volume of space, thus, even subtle changes of the drug height in the pore could significantly affect the REDOR dephasing.

Excess drug and other membrane composition changes are known to have significant effects on the conformational dynamics of M2TM.<sup>18,19,56,60</sup> For example, the addition of cholesterol at lower concentrations than the Rmt amount used here causes significant changes in the thermodynamic stability<sup>44</sup> and structure<sup>21</sup> of the protein. Relaxation NMR data revealed that the uniaxial diffusion of M2TM tetramers in DLPC bilayers was sped up by excess Amt in the membrane,<sup>61</sup> suggesting that the tetramers adopt tighter conformations due to the indirect influence of the drug on the membrane fluidity. Thus, the first equivalent of Rmt may be bound deeper in the pore, with the ethylamine outside the detectable ( $\sim 5$  Å) distance range of Gly34. As excess Rmt partitioned into the membrane, the tetramers may tighten slightly, pushing the drug up in the channel so that the  $\text{CD}_3$  group approached Gly34, giving measurable dipolar dephasing.

The downward orientation of the polar amine in the pore confirms that the adamantane drugs inhibit the M2 proton channel activity not only by steric block and dehydration of the channel,<sup>22</sup> but also by indirect drug–His37 interactions. The C-terminus-pointing amine would be able to form hydrogen

bonds with the clusters of water molecules near His37.<sup>38</sup> These water-mediated H-bonds would tend to reduce the His37 pK<sub>a</sub> as shown for Amt-bound M2TM in <sup>15</sup>N chemical shift measurements.<sup>26</sup> The perturbation of His37 pK<sub>a</sub> is relevant to inhibition, because it increases the fraction of the protein in the high-pH form and decreases dynamic processes believed to be required for proton conduction.<sup>14,18,62–64</sup> In a new spiro-piperidine inhibitor of M2 with 10-fold higher potency than Amt, methyl substitution of the amine was found to reduce the potency significantly, indicating the importance of the polar moiety.<sup>53</sup>

## CONCLUSIONS

The solid-state and solution NMR results shown here collectively demonstrate that Rmt binds the M2TM channel in a very similar fashion to Amt. At the stoichiometric drug concentration, Rmt binds inside the pore with the molecular axis roughly parallel to the bilayer normal. The polar group points toward the C-terminus, supporting the notion that the drug inhibits the proton conductance not only by interrupting the water wire leading to His37,<sup>30,65</sup> but also by forming water-mediated H-bonds with His37, thus perturbing its pK<sub>a</sub>. The proximity of the methyl group to the Gly34 backbone also suggests that the higher affinity of Rmt for M2 than Amt<sup>66</sup> may result from better space filling of the drug in the channel and dehydration of the additional hydrophobic methylene and methyl groups. This insight suggests that new drugs to target resistant variants of the M2 protein may involve side groups that similarly access the space near Gly34. The dynamics of Rmt inside the pore suggests two possible strategies in the design of new M2 inhibitors. In one strategy, one can design molecules that better fill the channel, leading to molecules with high potency for not only the wild type but also the drug-resistant mutants V27A and L26F. Alternatively, one can also adopt the strategy of retaining the molecular dynamics as a potential mode of conformational stabilization. The new structural information obtained here has informed both strategies.

This study not only extends the previous structural findings of Amt to Rmt, but also provides unique information about the polar group direction, which was absent in all previous high-resolution structures of the M2 protein.<sup>1,15</sup> The fundamental similarity of Rmt and Amt in their binding locations, as well as subtle differences in their lipid interactions, provides a rare opportunity to examine the entire distribution of bound states, including the lipid-bound as well as protein-bound states. These data give essential information to test and improve molecular dynamics protocols for simulating the kinetic steps involved in binding a hydrophobic drug to a membrane protein receptor.

The fact that Amt binds specifically to the pore of M2TM in DPC micelles in solution and cause chemical shift changes that are consistent with the effects of drug on M2TM<sup>51,54</sup> and M2(18–60)<sup>23</sup> in lipid bilayers, but distinct from the effects of drug on M2(18–60) in DHPC micelles,<sup>16</sup> underscore the importance of the environment to the functional structure of the protein and the mutual influence that can exist between the protein and detergent micelles.<sup>35</sup> The high-resolution orientational structure of the cytoplasmic helix recently determined by solid-state NMR in lipid bilayers<sup>64</sup> differs significantly from the structure in DHPC micelles. How exactly the cytoplasmic helix affects specific drug binding in the TM pore in a detergent environment remains an open question for future investigation.

## ASSOCIATED CONTENT

**S Supporting Information.** Protocols of protein expression, NMR sample preparation and experimental conditions, and additional NMR spectra. This material is available free of charge via the Internet at <http://pubs.acs.org>.

## AUTHOR INFORMATION

### Corresponding Author

mhong@iastate.edu; degradowf@gmail.com

## ACKNOWLEDGMENT

The authors thank Anjali Dike for measuring preliminary solution NMR spectra and Guy Montelione for NMR time on the Varian 600 MHz NMR spectrometer. This work is supported by NIH grants GM088204 to M.H. and GM56423 and AI74571 to W.F.D.

## REFERENCES

- (1) Cady, S. D.; Luo, W. B.; Hu, F. H.; Hong, M. *Biochemistry* **2009**, 48, 7356–7364.
- (2) Pinto, L. H.; Lamb, R. A. *J. Biol. Chem.* **2006**, 281, 8997–9000.
- (3) Gannagé, M.; Dormann, D.; Albrecht, R.; Dengjel, J.; Torossi, T.; Rämer, P. C.; Lee, M.; Strowig, T.; Arrey, F.; Conenello, G.; Pypaert, M.; Andersen, J.; García-Sastre, A.; Münz, C. *Cell Host Microbe* **2009**, 6, 367–380.
- (4) Schroeder, C. *Subcell. Biochem.* **2010**, 51, 77–108.
- (5) Rossman, J. S.; Jing, X.; Leser, G. P.; Balannik, V.; Pinto, L. H.; Lamb, R. A. *J. Virol.* **2010**, 84, 5078–5088.
- (6) Rossman, J. S.; Jing, X.; Leser, G. P.; Lamb, R. A. *Cell* **2010**, 142, 902–913.
- (7) Ma, C.; Polishchuk, A. L.; Ohigashi, Y.; Stouffer, A. L.; Schön, A.; Magavern, E.; Jing, X.; Lear, J. D.; Freire, E.; Lamb, R. A.; DeGrado, W. F.; Pinto, L. H. *Proc. Natl. Acad. Sci. U.S.A.* **2009**, 106, 12283–12288.
- (8) Park, E. K.; Castrucci, M. R.; Portner, A.; Kawaoka, Y. *J. Virol.* **1998**, 72, 2449–2455.
- (9) McCown, M. F.; Pekosz, A. *J. Virol.* **2006**, 80, 8178–8189.
- (10) Ohigashi, Y.; Ma, C.; Jing, X.; Balannik, V.; Pinto, L. H.; Lamb, R. A. *Proc. Natl. Acad. Sci. U.S.A.* **2009**, 106, 18775–18779.
- (11) Balannik, V.; Carnevale, V.; Fiorin, G.; Levine, B. G.; Lamb, R. A.; Klein, M. L.; DeGrado, W. F.; Pinto, L. H. *Biochemistry* **2010**, 49, 696–708.
- (12) Jing, X.; Ma, C.; Ohigashi, Y.; Oliveira, F. A.; Jardetzky, T. S.; Pinto, L. H.; Lamb, R. A. *Proc. Natl. Acad. Sci. U.S.A.* **2008**, 105, 10967–10972.
- (13) Wang, C.; Takeuchi, K.; Pinto, L. H.; Lamb, R. A. *J. Virol.* **1993**, 67, 5585–5594.
- (14) Stouffer, A. L.; Acharya, R.; Salom, D.; Levine, A. S.; Di Costanzo, L.; Soto, C. S.; Tereshko, V.; Nanda, V.; Stayrook, S.; DeGrado, W. F. *Nature* **2008**, 451, 596–599.
- (15) Cady, S. D.; Schmidt-Rohr, K.; Wang, J.; Soto, C. S.; DeGrado, W. F.; Hong, M. *Nature* **2010**, 463, 689–692.
- (16) Schnell, J. R.; Chou, J. J. *Nature* **2008**, 451, 591–595.
- (17) Rosenberg, M. R.; Casarotto, M. G. *Proc. Natl. Acad. Sci. U.S.A.* **2010**, 107, 13866–13871.
- (18) Hu, F.; Luo, W.; Cady, S. D.; Hong, M. *Biochim. Biophys. Acta* **2010**, 1808, 415–423.
- (19) Li, C.; Qin, H.; Gao, F. P.; Cross, T. A. *Biochim. Biophys. Acta* **2007**, 1768, 3162–3170.
- (20) Stouffer, A. L.; Nanda, V.; Lear, J. D.; DeGrado, W. F. *J. Mol. Biol.* **2005**, 347, 169–179.
- (21) Luo, W.; Cady, S. D.; Hong, M. *Biochemistry* **2009**, 48, 6361–6368.
- (22) Luo, W.; Hong, M. *J. Am. Chem. Soc.* **2010**, 132, 2378–2384.

- (23) Andreas, L. B.; Eddy, M. T.; Pielak, R. M.; Chou, J. J.; Griffin, R. G. *J. Am. Chem. Soc.* **2010**, *132*, 10958–10960.
- (24) Chaudhury, S.; Gray, J. J. *J. Mol. Biol.* **2008**, *381*, 1068–1087.
- (25) Ma, B. Y.; Kumar, S.; Tsai, C. J.; Nussinov, R. *Protein Eng.* **1999**, *12*, 713–720.
- (26) Hu, J.; Fu, R.; Cross, T. A. *Biophys. J.* **2007**, *93*, 276–283.
- (27) Hu, J.; Fu, R.; Nishimura, K.; Zhang, L.; Zhou, H. X.; Busath, D. D.; Vijayvergiya, V.; Cross, T. A. *Proc. Natl. Acad. Sci. U.S.A.* **2006**, *103*, 6865–6870.
- (28) Wang, C.; Lamb, R. A.; Pinto, L. H. *Biophys. J.* **1995**, *69*, 1363–1371.
- (29) Sansom, M. S. P.; Kerr, I. D. *Protein Eng.* **1993**, *6*, 65–74.
- (30) Chen, H.; Wu, Y.; Voth, G. A. *Biophys. J.* **2007**, *93*, 3470–3479.
- (31) Yi, M.; Cross, T. A.; Zhou, H. X. *J. Phys. Chem. B* **2008**, *112*, 7977–7979.
- (32) Intharathep, P.; Laohpongspaisan, C.; Rungrotmongkol, T.; Loisruangsin, A.; Malaisree, M.; Decha, P.; Aruksakunwong, O.; Chuenpennit, K.; Kaiyawet, N.; Sompornpisut, P.; Pianwanit, S.; Hannongbua, S. *J. Mol. Graphics Modell.* **2008**, *27*, 342–348.
- (33) Chuang, G. Y.; Kozakov, D.; Brenke, R.; Beglov, D.; Guarnieri, F.; Vajda, S. *Biophys. J.* **2009**, *97*, 2846–2853.
- (34) Laohpongspaisan, C.; Rungrotmongkol, T.; Intharathep, P.; Malaisree, M.; Decha, P.; Aruksakunwong, O.; Sompornpisut, P.; Hannongbua, S. *J. Chem. Inf. Model.* **2009**, *49*, 847–852.
- (35) Poget, S. F.; Girvin, M. E. *Biochim. Biophys. Acta* **2007**, *1768*, 3098–3106.
- (36) Tobler, K.; Kelly, M. L.; Pinto, L. H.; Lamb, R. A. *J. Virol.* **1999**, *73*, 9695–9701.
- (37) Pielak, R. M.; Schnell, J. R.; Chou, J. J. *Proc. Natl. Acad. Sci. U.S.A.* **2009**, *106*, 7379–7384.
- (38) Acharya, A.; Carnevale, V.; Fiorin, G.; Levine, B. G.; Polishchuk, A.; Balannick, V.; Samish, I.; Lamb, R. A.; Pinto, L. H.; DeGrado, W. F.; Klein, M. L. *Proc. Natl. Acad. Sci. U.S.A.* **2010**, *107*, 15075–15080.
- (39) Howard, K. P.; Lear, J. D.; DeGrado, W. F. *Proc. Natl. Acad. Sci. U.S.A.* **2002**, *99*, 8568–8572.
- (40) Kochendoerfer, G. G.; Salom, D.; Lear, J. D.; Wilk-Orescan, R.; Kent, S. B.; DeGrado, W. F. *Biochemistry* **1999**, *38*, 11905–11913.
- (41) Salom, D.; Hill, B. R.; Lear, J. D.; DeGrado, W. F. *Biochemistry* **2000**, *39*, 14160–14170.
- (42) Stouffer, A. L.; Ma, C.; Cristian, L.; Ohigashi, Y.; Lamb, R. A.; Lear, J. D.; Pinto, L. H.; DeGrado, W. F. *Structure* **2008**, *16*, 1067–1076.
- (43) Stouffer, A. L.; DeGrado, W. F.; Lear, J. D. *Prog. Colloid Polym. Sci.* **2006**, *131*, 108–115.
- (44) Cristian, L.; Lear, J. D.; DeGrado, W. F. *Proc. Natl. Acad. Sci. U.S.A.* **2003**, *100*, 14772–14777.
- (45) Cristian, L.; Lear, J. D.; DeGrado, W. F. *Protein Sci.* **2003**, *12*, 1732–1740.
- (46) Astrahan, P.; Kass, I.; Cooper, M. A.; Arkin, I. T. *Proteins: Struct., Funct., Bioinf.* **2004**, *55*, 251–257.
- (47) Nguyen, P. A.; Soto, C. S.; Polishchuk, A.; Caputo, G. A.; Tatko, C. D.; Ma, C.; Ohigashi, Y.; Pinto, L. H.; DeGrado, W. F.; Howard, K. P. *Biochemistry* **2008**, *47*, 9934–9936.
- (48) Sharma, M.; Yi, M.; Dong, H.; Qin, H.; Peterson, E.; Busath, D.; Zhou, H. X.; Cross, T. A. *Science* **2010**, *330*, 509–512.
- (49) Kanelis, V.; Forman-Kay, J. D.; Kay, L. E. *IUBMB Life* **2001**, *52*, 291–302.
- (50) Delaglio, F.; Grzesiek, S.; Vuister, G. W.; Zhu, G.; Pfeifer, J.; Bax, A. *J. Biomol. NMR* **1995**, *6*, 277–293.
- (51) Cady, S. D.; Mishanina, T. V.; Hong, M. *J. Mol. Biol.* **2009**, *385*, 1127–1141.
- (52) Vold, R. L.; Hoatson, G. L. *J. Magn. Reson.* **2009**, *198*, 57–72.
- (53) Wang, J.; Cady, S. D.; Balannik, V.; Pinto, L. H.; DeGrado, W. F.; Hong, M. *J. Am. Chem. Soc.* **2009**, *131*, 8066–8076.
- (54) Cady, S. D.; Hong, M. *Proc. Natl. Acad. Sci. U.S.A.* **2008**, *105*, 1483–1488.
- (55) Hong, M.; Doherty, T. *Chem. Phys. Lett.* **2006**, *432*, 296–300.
- (56) Cady, S. D.; Goodman, C.; Tatko, C.; DeGrado, W. F.; Hong, M. *J. Am. Chem. Soc.* **2007**, *129*, 5719–5729.
- (57) Lange, O. F.; Lakomek, N. A.; Farès, C.; Schröder, G. F.; Walter, K. F.; Becker, S.; Meiler, J.; Grubmüller, H.; Griesinger, C.; de Groot, B. L. *Science* **2008**, *320*, 1471–1475.
- (58) Jaroniec, C. P.; Toung, B. A.; Herzfeld, J.; Griffin, R. G. *J. Am. Chem. Soc.* **2001**, *123*, 3507–3519.
- (59) Li, C.; Yi, M.; Hu, J.; Zhou, H. X.; Cross, T. A. *Biophys. J.* **2008**, *94*, 1295–1302.
- (60) Duong-Ly, K. C.; Nanda, V.; DeGrado, W. F.; Howard, K. P. *Protein Sci.* **2005**, *14*, 856–61.
- (61) Cady, S. D.; Hong, M. *J. Biomol. NMR* **2009**, *45*, 185–196.
- (62) Khurana, E.; Dal Peraro, M.; DeVane, R.; Vemparala, S.; DeGrado, W. F.; Klein, M. L. *Proc. Natl. Acad. Sci. U.S.A.* **2009**, *106*, 1069–1074.
- (63) Yi, M.; Cross, T. A.; Zhou, H. X. *Proc. Natl. Acad. Sci. U.S.A.* **2009**, *106*, 13311–13316.
- (64) Hu, F.; Luo, W.; Hong, M. *Science* **2010**, *330*, 505–509.
- (65) Sansom, M. S. P.; Kerr, I. D.; Smith, G. R.; Son, H. S. *Virology* **1997**, *233*, 163–173.
- (66) Balannik, V.; Wang, J.; Ohigashi, Y.; Jing, X.; Magavern, E.; Lamb, R. A.; DeGrado, W. F.; Pinto, L. H. *Biochemistry* **2009**, *48*, 11872–11882.

## Supporting information

### Specific Binding of Adamantane Drugs and Direction of their Polar Amines in the Pore of the Influenza M2 Proton Channel in Lipid Bilayers and Dodecylphosphocholine Micelles Determined by NMR Spectroscopy

Sarah D. Cady<sup>1</sup>, Jun Wang<sup>2</sup>, Yibing Wu<sup>2</sup>, William F. DeGrado<sup>2\*</sup>, and Mei Hong<sup>1\*</sup>

*Expression and trypsin digestion of U-<sup>15</sup>N and U-<sup>15</sup>N-<sup>13</sup>C labeled M2TM(19-49) for detergent screening of solution NMR*

BL21(DE3)pLyS E. Coli cells with pET23D(+) plasmids containing the Udorn wt M2 gene were grown in LB agar plates with 100 µg/ml ampicilin at 37°C overnight. A single colony was picked up from the plate to inoculate 5ml LB supplemented with 100 µg/ml ampicilin, and was allowed to incubate at 37°C with 200rpm shaking for 8hrs. Next, 0.5 ml of the above cell solution was used to inoculate 50ml of minimal media with 1g/L <sup>15</sup>NH<sub>4</sub>Cl, 4g/L glucose and 100 µg/ml ampicilin and shake at 37°C overnight (for double <sup>15</sup>N and <sup>13</sup>C labeling, the minimal media was supplemented with 1g/L <sup>15</sup>NH<sub>4</sub>Cl, 4g/L <sup>13</sup>C glucose). The overnight culture was used to inoculate 1 L of minimal media with 1g/L <sup>15</sup>NH<sub>4</sub>Cl and 100 µg/ml ampicilin. When OD<sub>600</sub> reached 0.7-1.0 (normally after 3hrs), M2 expression was induced with 1 mM IPTG (final concentration). Protein expression was halted three hours later by centrifugation at 4°C for 30 min. The cell pellet was resuspended in 50 ml of 50 mM Tris (pH 8), 40 mM OG, 150 mM NaCl, 0.25 µg/ml lysozyme, 0.02 µg/ml DNase I and 500 µM PMSF at 0°C. The mixture was sonicated on ice for 20 min (20% amplitude, 1 s on 1 s off), followed by further reconstitution using a homogenizer for 10 mins to make the solution homogeneous. The solution was then centrifuged at 15,000 g for 30 mins. The supernatant was saved for Ni-NTA column purification, and the pellet was subjected to another round of reconstitution as described above. Finally the supernatants from two rounds were combined and incubated with 10 ml Ni-NTA super flow resin (Qiagen) and 20 mM imidazole at room temperature for 30 min with gentle shaking. The column was washed successively with 50 mM Tris (pH 8), 150 mM NaCl, 40 mM OG, 20% v/v

glycerol, then 50 mM Tris (pH 8), 20 mM OG, 20% v/v glycerol, followed by 50 mM Tris (pH 8), 4 mM OG, 20% v/v glycerol, 20 mM imidazole. Finally, the M2 protein was eluted with 50 mM Tris (pH 8), 4 mM OG, 20% v/v glycerol, 300 mM imidazole. The purity of M2 was judged by gel electrophoresis and HPLC to be >95%. Full length M2 was digested by TPCK-trypsin (Thermo Fisher, cat # PI-20233, 10mg/ml) in the elution buffer overnight at 37°C. The resulting solution was separated by C4 reverse phase HPLC with linear gradient of 70% B' to 95% B' (Eluent A: 89.9% H<sub>2</sub>O + 10% isopropanol + 0.1% TFA; Eluent B: 59.9% isopropanol + 30% acetonitrile + 10% H<sub>2</sub>O + 0.1% TFA) to give two major fragments M2(19-49) and M2(19-53) in 3:2 ratio. ESI-MS of the A/M2(19-49) was found to be 3507.2411, calculated 3505.8149.

*Chemical shift assignment of <sup>15</sup>N, <sup>13</sup>C-V27, A30, G34-labeled M2TM(22-46) in the absence and presence of Amt and Rmt*

Val, Ala and Gly have characteristic <sup>13</sup>C $\alpha$  chemical shifts of 62.4 ± 2.9 ppm, 53.2 ± 2.0 ppm, and 45.3 ± 1.3 ppm, respectively, thus the backbone C $\alpha$  signals can be unambiguously assigned in the <sup>13</sup>C HSQC spectra. The Val C $\beta$  chemical shift should be 32.7 ± 1.8 ppm, and is also straightforward to assign. The methyl carbon and protons of Ala are usually shifted upfield by 2.2 ppm and downfield by 0.5 ppm, respectively, compared to the corresponding atoms of Val, so the assignment of the methyl group is also clear. The 2D H(N)CA experiment correlates the amide <sup>1</sup>H chemical shifts with the intra-residue and preceding residue <sup>13</sup>C chemical shifts. Since the preceding residues of V27, A30 and G34 are unlabeled, the H(N)CA experiments only connect the intra-residue amide <sup>1</sup>H and <sup>13</sup>C chemical shifts. The 2D (H)C(C)H TOCSY experiment was used to extend and confirm the <sup>1</sup>H and <sup>13</sup>C assignments within a spin system. The C $\alpha$  peak of G34 was too weak to observe, which may be due to high dynamics, as supported by the weak signals of G34 in both the <sup>13</sup>C and <sup>15</sup>N HSQC spectra. Nevertheless, G34 assignment was obvious after the other two residues had been assigned and because Gly <sup>15</sup>N resonates in a very unique region of the spectrum (109.7 ± 4.0 ppm). Figure S7A-C show the assignments of M2TM in the apo state and in the presence of Amt and Rmt.

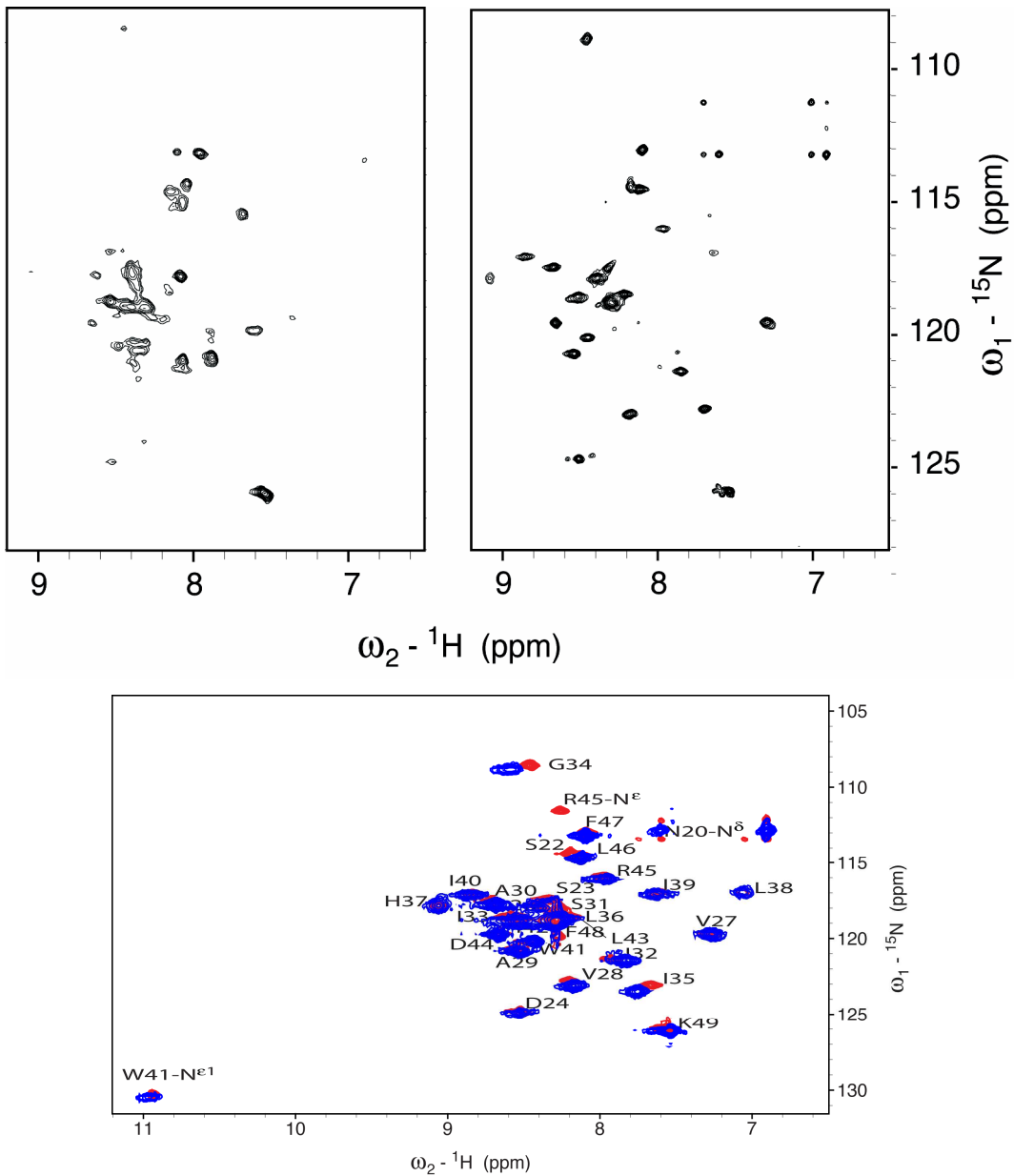


**Figure S1.** The top panels show 2D <sup>15</sup>N TROSY-HSQC spectra of 1 mM <sup>15</sup>N uniformly labeled M2TM(19-49) in the absence (left) and presence (right) of 5 eq Amt, at 313 K in 50 mM DPC (50 mM sodium phosphate in 10% D<sub>2</sub>O and 90% H<sub>2</sub>O). The spectra were measured on a Varian INOVA 600 MHz (left) and 900 MHz (right) spectrometer equipped with a <sup>1</sup>H{<sup>13</sup>C, <sup>15</sup>N}-triple resonance cryoprobe. Similar to the spectra in **Fig. 1**, upon Amt binding, <sup>1</sup>H chemical shift dispersion increases, and peak shape and linewidths become more uniform, indicating the drug-protein complex adopts a well-structured conformation. The bottom panel shows a comparison

of TROSY-HSQC spectrum acquired for  $^{15}\text{N}$  uniformly labeled M2TM (19-49) in the presence of 10 equivalent WJ10 per tetramer (Red) with 1: 100 protein : DPC, and 5 equivalent Rmt per tetramer (Blue) with 1: 50 protein : DPC , at 313K, 50 mM Na phosphate in 10%  $\text{D}_2\text{O}$  and 90%  $\text{H}_2\text{O}$ . Except slight shifting of residues G34 and I35, the two spectra superimpose.

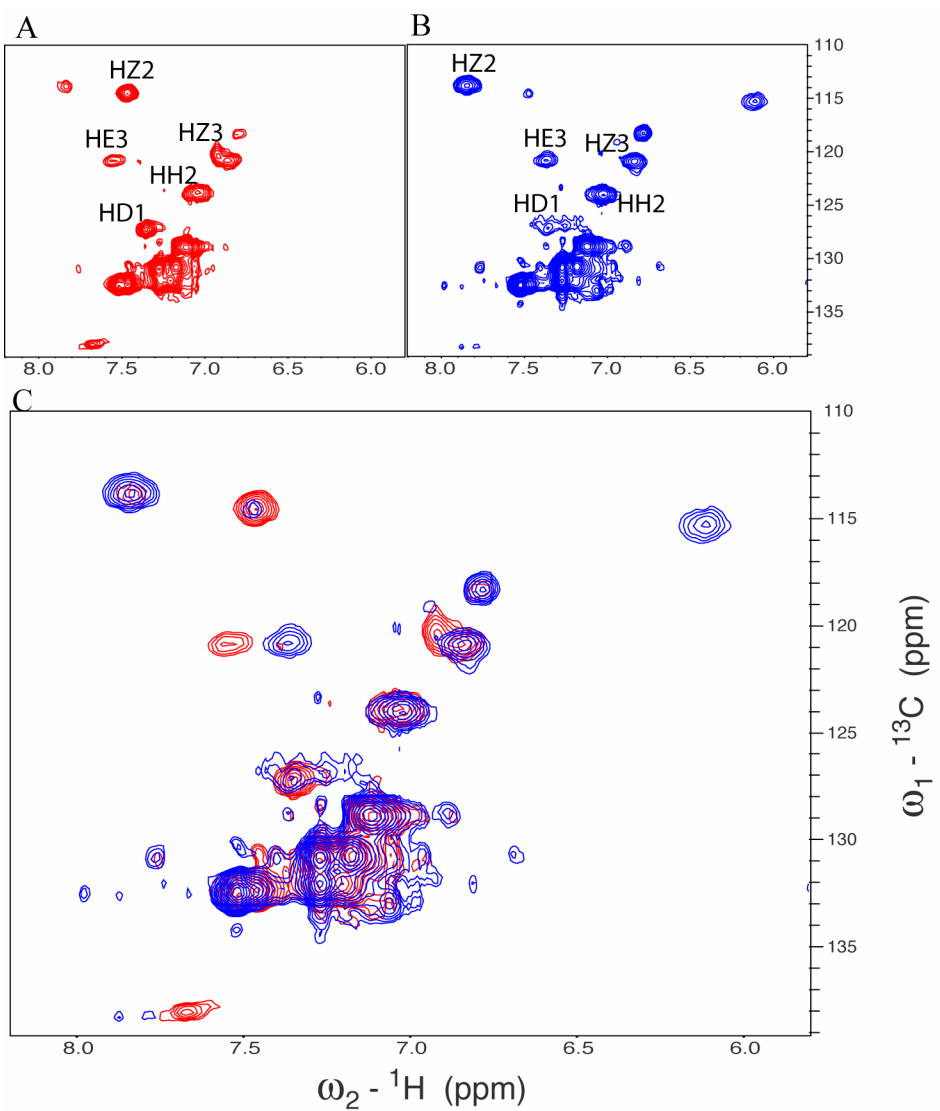


**Figure S2.** Aromatic  ${}^{13}\text{C}$  HSQC spectrum of M2TM(19-49) in the absence of the inhibitor WJ10 (red, A) shows two conformers for W41, one much stronger than the other. Addition of WJ10 (blue, B) shifts the equilibrium towards the one less populated in the apo state. Superposition of the two spectra (C) clearly indicates that there are no additional new peaks for W41. The assignments of the W41 indole ring were based on 2D  ${}^1\text{H}$  NOESY spectra recorded in  $\text{H}_2\text{O}$  and  $\text{D}_2\text{O}$  (unpublished data). The sample was the same as described in Fig. 1 of the main text.

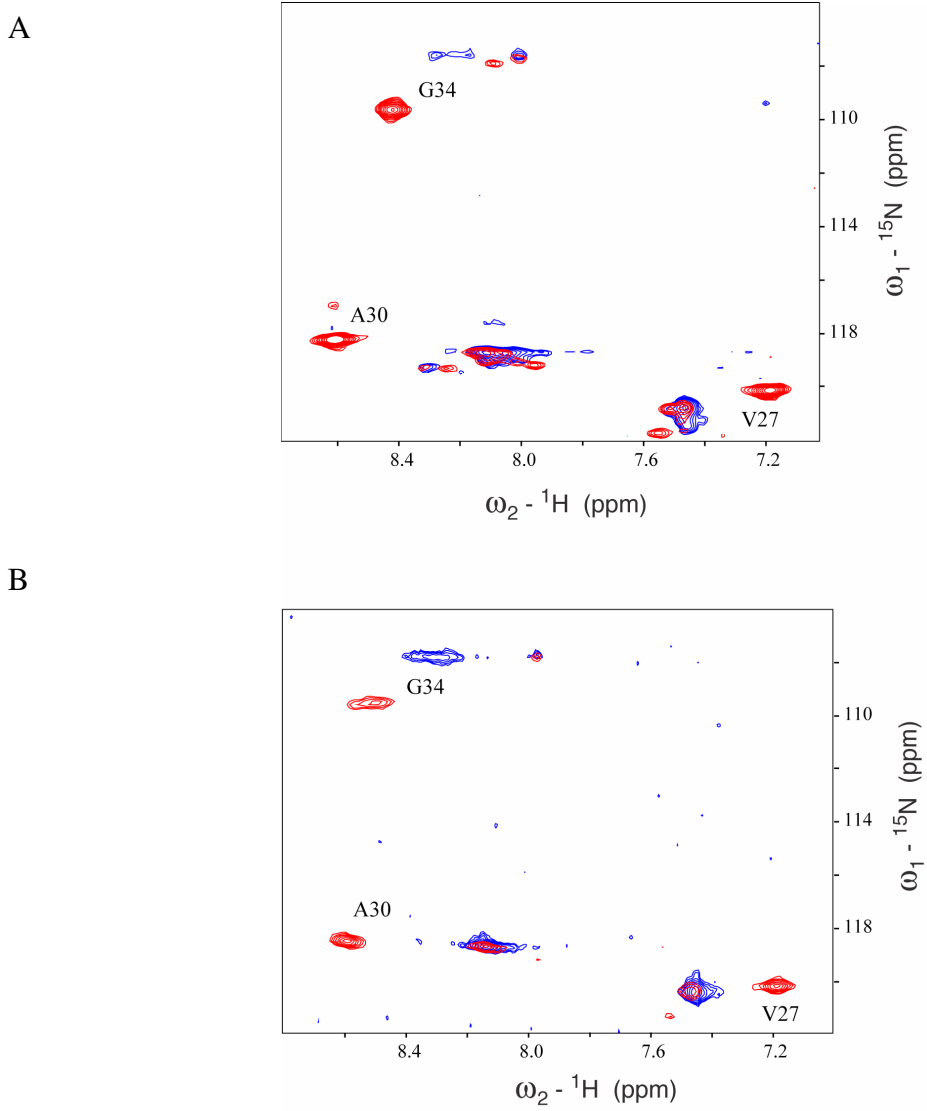


**Figure S3.** Overlay of  $^{15}\text{N}$  TROSY HSQC spectra of VAG-M2TM(22-46) in the absence (blue) and presence (red) of Amt (A) and Rmt (B) to illustrate the perturbation of the backbone conformation by drugs.  $^1\text{H}$  chemical shift changes for all three residues ranged from 0.2 to 0.5 ppm upon drug binding, showing the drug strongly perturbs pore-lining residues. Lineshape and intensity analysis shows that drug-bound peaks of the three residues are more uniform than the unbound peaks, indicating that the bound conformation is more homogeneous. The spectra were recorded on a 500 MHz and a 600 MHz spectrometer. The peptide was reconstituted at 1 : 100 peptide/DPC, pH 7.5 (50 mM sodium phosphate buffer), 313 K, and 2 mM peptide.

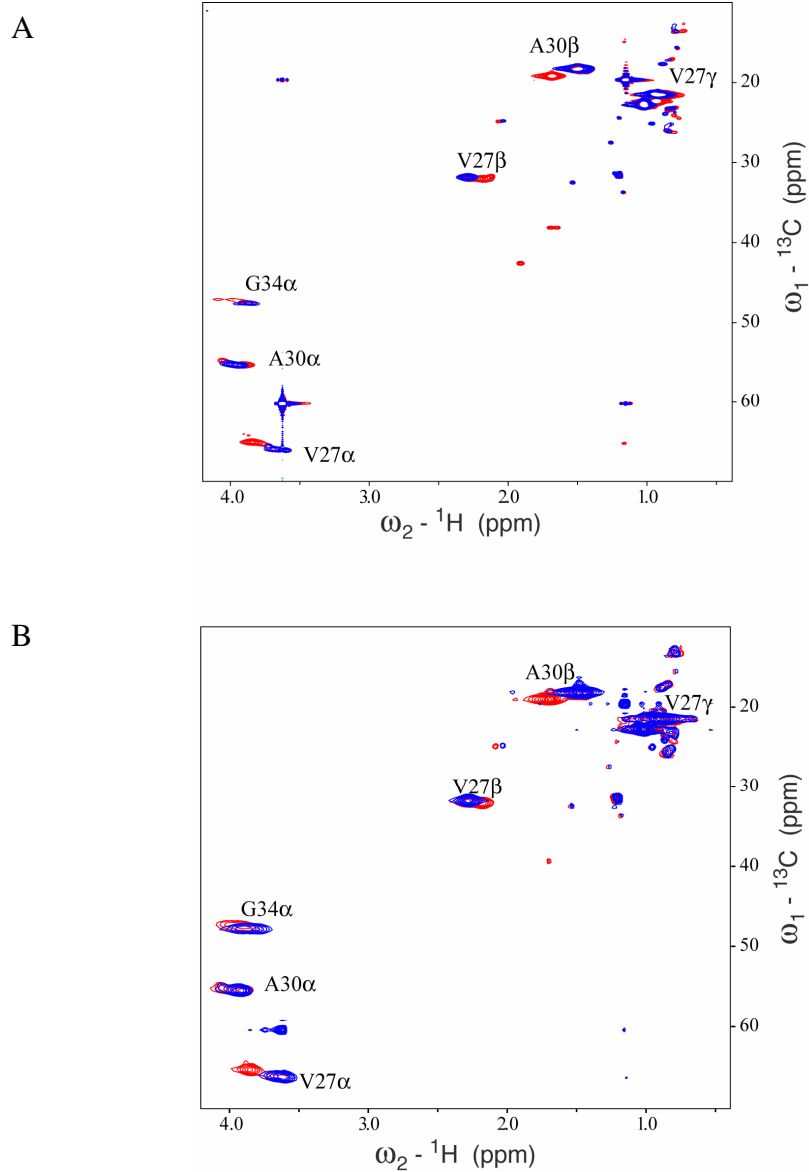


**Figure S4.** Overlay of  $^{13}\text{C}$  HSQC spectra of VAG-M2TM(22-46) in the absence (blue) and presence (red) of Amt (A) and Rmt (B) to illustrate perturbation of the sidechain conformation by drugs. Chemical shifts are very similar for all peaks of the two bound forms, suggesting similar geometry of the complexes. The peptide was reconstituted at 1 : 100 peptide/DPC, pH 7.5 (50 mM sodium phosphate buffer), 313 K, and 2 mM peptide.

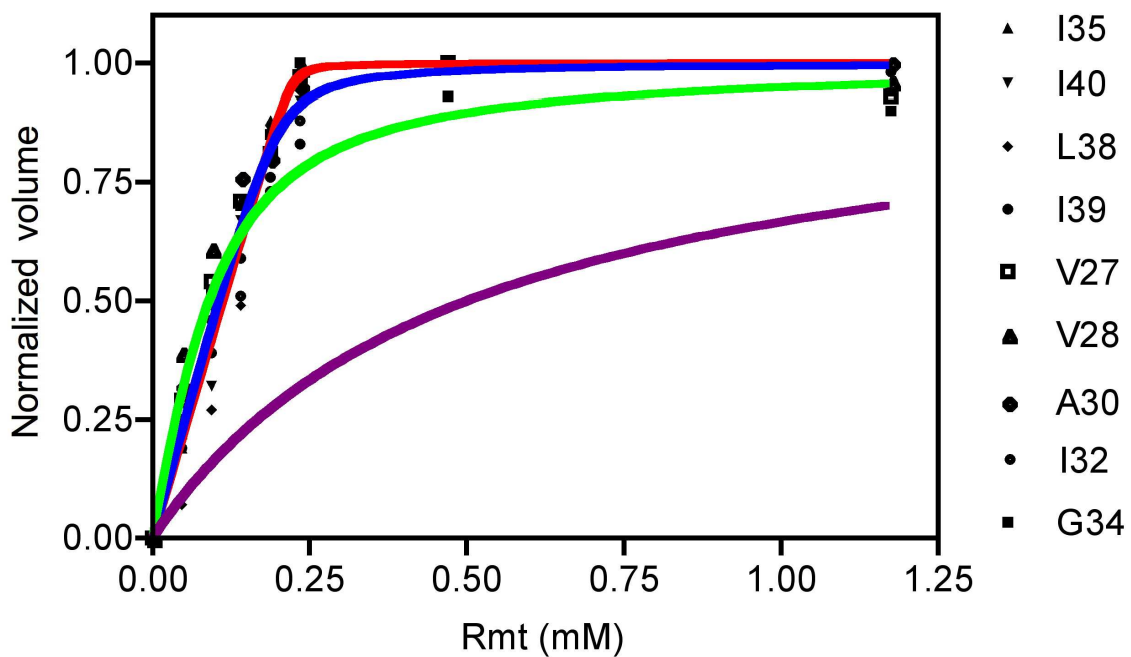


**Figure S5.** Analysis of the titration data from **Fig. 2** of the main text. The dissociation constant was held at various values by setting  $K_D$  as 0.5  $\mu\text{M}$  (red), 5  $\mu\text{M}$  (Blue), 50  $\mu\text{M}$  (Green) and 500  $\mu\text{M}$  (Purple), respectively. The resulting values of N and fitting statistics are shown below in **Table S1**. Satisfactory fits were obtained with N in the range of 0.88 to 0.94 and  $K_D$  less than or equal to 5  $\mu\text{M}$ . The quality of the fit deteriorated for  $K_D$  greater than 5  $\mu\text{M}$ .

**Table S1:** Statistics of fittings shown in the **Fig.2** and **Fig.S5** for the titration data.

Best-fit Values							
N	$0.88 \pm 0.04$	1 <sup>a</sup>	4 <sup>a</sup>	$0.94 \pm 0.02$	$0.86 \pm 0.02$	$0.34 \pm 0.05$	$0.0 \pm 0.41$
K <sub>D</sub> ( $\mu\text{M}$ )	$3.9 \pm 1.7$	$0.0 \pm 74$	$0.0 \pm 4.4 \times 10^2$	0.5 <sup>a</sup>	5 <sup>a</sup>	50 <sup>a</sup>	500 <sup>a</sup>
R <sup>2</sup>	0.97	0.96	-0.55	0.96	0.96	0.91	-0.34
Absolute sum of squares	0.31	0.40	14	0.34	0.31	0.76	12

a: Values fixed in the fitting.

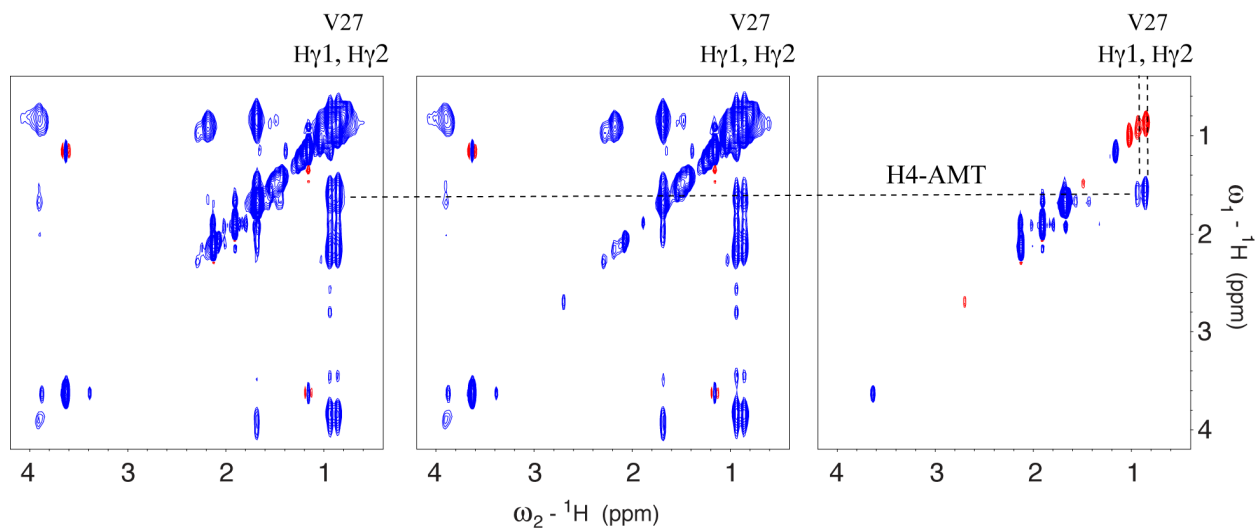
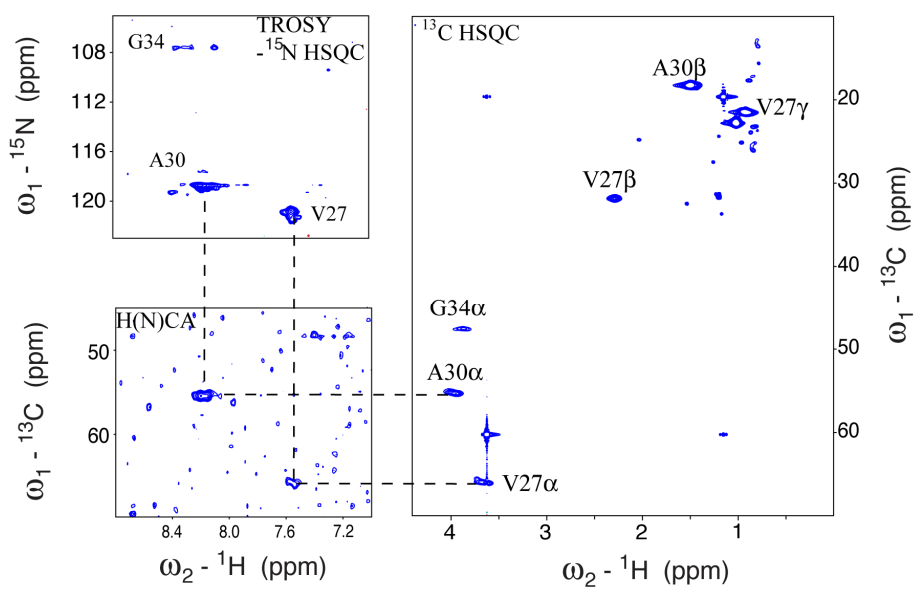
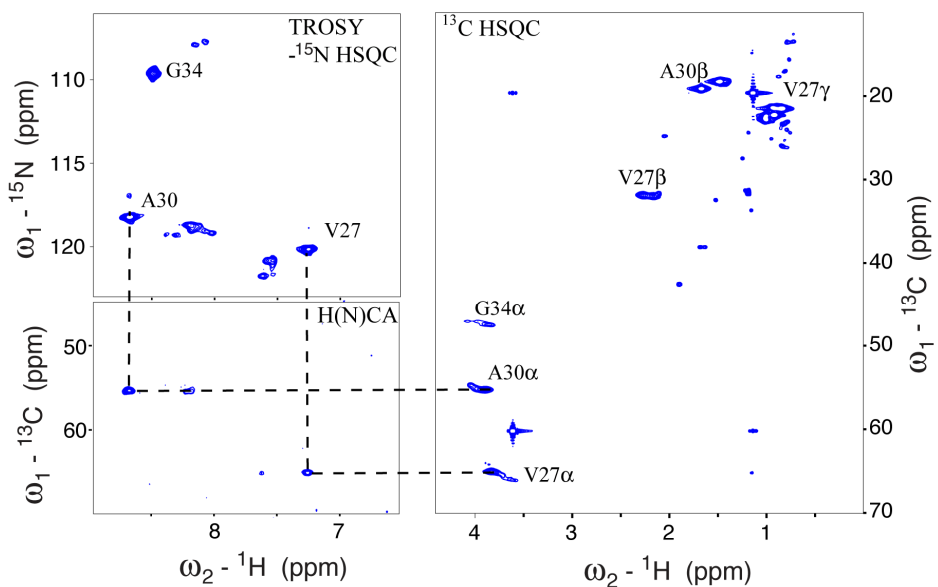


**Figure S6.** Amantadine remains bound in the pore in the presence of a large excess of drug, as assessed from intermolecular NOEs detected in the difference spectrum. The upfield region of the 2D (<sup>13</sup>C)-edited NOESY spectrum (200 ms mixing time) of M2TM with 20 eq protonated Amt (left) and deuterated Amt (middle) at 313 K gave rise to a difference spectrum (right) that shows the same intermolecular NOEs between Val27 and the drug as when the drug was present at much lower molar excess (Fig. 2).

A



B



C

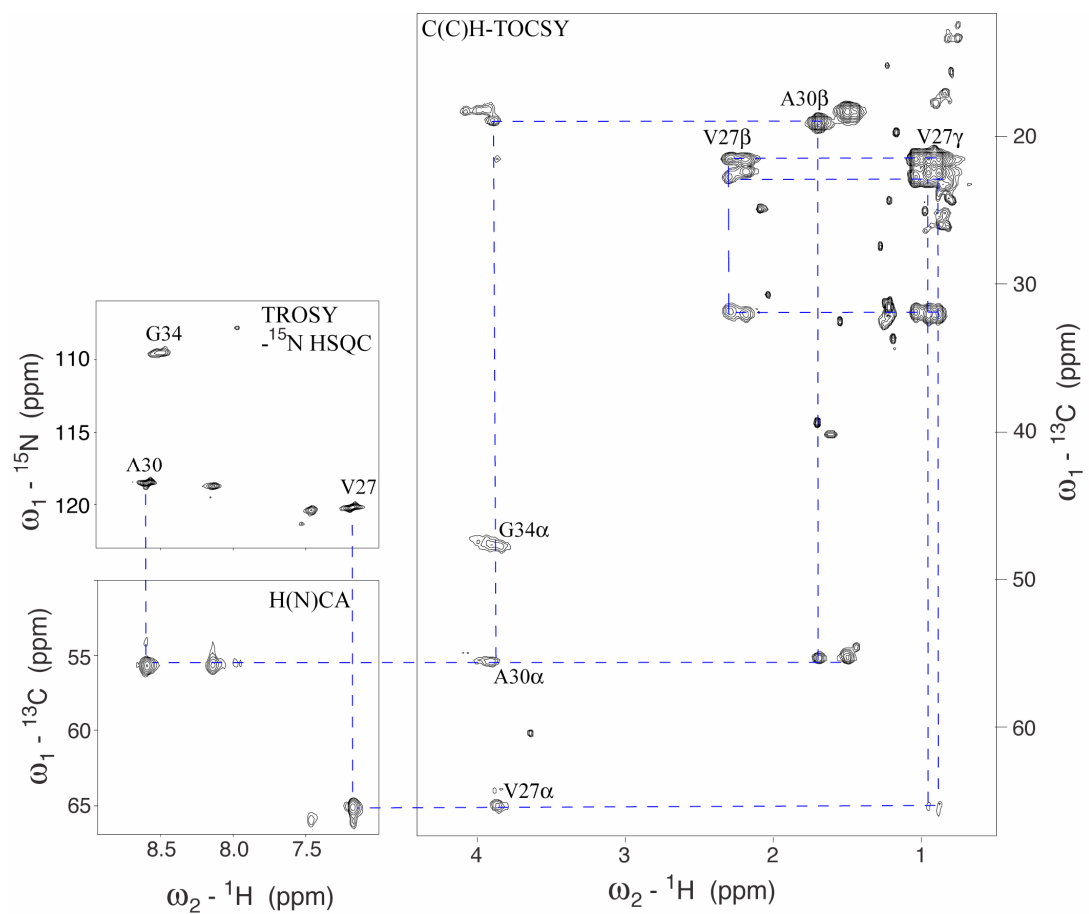


**Figure S7.** Chemical shift assignment of VAG-M2TM(22-46) in DPC micelles. (A) In the absence of drug. (B) Bound with Amt. (C) Bound with Rmt. The peptide was reconstituted at 1 : 100 peptide/DPC, pH 7.5 (50 mM sodium phosphate buffer in 10% D<sub>2</sub>O, 90% H<sub>2</sub>O), 313 K, 2 mM peptide (monomer concentration), and 1 mM Amt or Rmt.